



Comparing seismic performances of single-span RC frames with and without wing wall retrofitting by shaking table tests

Lingxin Zhang ^{a,b}, Caiquan Wang ^c, Yongsheng Chen ^{a,b,*}

^a Key Laboratory of Earthquake Engineering and Engineering Vibration, Institute of Engineering Mechanics, China Earthquake Administration, Harbin, 150080, China

^b Key Laboratory of Earthquake Disaster Mitigation, Ministry of Emergency Management, Harbin, 150080, China

^c The Architectural Design & Research Institute of Zhejiang University Co., Ltd, Hangzhou, 310000, China



ARTICLE INFO

Keywords:

Shaking table test
Wing wall retrofit
Single-span frame
Similarity law
Dynamic response

ABSTRACT

It is necessary to retrofit existing single-span reinforced concrete (RC) frames which could not meet the current seismic codes due to lack of multiple seismic lines of defence. Adding wing wall is one of the retrofit method that can improve the redundancy of single-span RC frames. To study the effectiveness of single-span frames retrofitted by wing walls, shaking table tests were conducted on two 1:5 specimens to compare the seismic behaviour of single-span RC frames with and without wing wall retrofitting. First, a retrofit scheme for the frame using wing walls was selected. Two specimens—a single-span RC frame and an identical frame with a wing wall retrofit—were placed on the same shaking table board and tested simultaneously. Contrast tests were conducted for 20 earthquake cases. The main conclusions are as follows: (1) Adding wing walls to a single-span frame in bi-direction is a reasonable strengthening scheme. (2) For the single-span frame without retrofitting, cracks appeared in the early stages and rapidly developed, forming plastic hinges at the ends of the beams and columns. For the single-span frame with retrofitting, cracks first appeared in the construction joints between the wing walls and beams, and then extended to wing walls and beams. The test phenomena indicate that adding wing walls to a single-span frame can increase system redundancy, and act as the first anti-seismic line of defence. (3) From the measured data, it is shown that adding wing walls to a single-span frame can improve its seismic capacity and control the lateral deformation. The peak floor displacement response of the retrofitted frame reduced by 30%–40% compare with that of the frame without retrofitting. (4) When input PGA was 0.15g (design based earthquake), slight damage occurred to the frame retrofitted by wing wall, while damage of the frame without retrofitting was moderate. When input PGA was 0.30g (rare earthquake), moderate damage occurred to the frame retrofitted by wing wall, while damage of frame without retrofitting was severe. Therefore, adding wing walls is an effective method for retrofitting single-span RC frame structures.

1. Introduction

Single-span reinforced concrete (RC) frames that satisfy lighting and ventilation requirements are widely used as structural forms for primary and secondary school buildings in Southern China. During recent major earthquakes (Chi-Chi, 1999; Wenchuan, 2008), buildings of this structural form suffered serious damage owing to deficiencies in their seismic capacity, especially single-span RC

* Corresponding author. Institute of Engineering Mechanics, China Earthquake Administration, No. 29 Xuefu Road, Nangang District, Harbin, 150080, China.
E-mail address: chenys@iem.ac.cn (Y. Chen).

frames with a cantilevered corridor [1,2]. After the Wenchuan Earthquake, school buildings were classified as *Importance* in the seismic fortification category [3], and they were strictly prohibited from adopting the structural form of a single-span RC frame in the revised code for seismic design of buildings in China [4]. In addition, the new code highlights the necessity of seismic assessment and retrofitting of existing single-span RC-frame school buildings. The necessity also indicated in the 2022 Luding earthquake (Ms 6.8), in which an abandoned single-span teaching building was severely damaged, as shown in Fig. 1. However, two multi-span frame kindergartens constructed following the new code were almost intact, although they were located in the same intensity zone [5]. Therefore, existing single-span school buildings built according to the old code are urgent to be retrofitted to improve their seismic performance and prevent serious damage during earthquakes.

A single-span RC frame, designed strictly according to the latest Code for Seismic Design of Buildings in China, guarantees sufficient bearing capacity, rigidity, and strength. The problem with this type of building structure lies in the design concept, such as the deficiency in structural redundancy and multiple anti-seismic lines of defence. Retrofit methods for existing single-span RC frames should focus on increasing the statically indeterminate degrees and enhancing the extra seismic fortification line. There are many retrofit methods, such as installing braces, increasing columns or their cross sections, enveloping steel, and retrofitting with carbon fibre sheets. Compared with other retrofit methods such as installing diagonal braces and setting columns in the corridor, adding a wing wall presents several advantages such as low disturbance, flexible arrangement, convenient installation, and reasonable conceptual design. This retrofit method was proven during the 1999 Chi-Chi earthquake, in which a school building retrofitted with RC wing walls performed quite well and exhibited only minor damage. Therefore, adding wing walls has been adopted by engineers in China as a practical retrofit method [6].

A number of static tests and corresponding analyses on a single column with a wing wall have been reported in the literature [7–16]. These studies showed that wing walls can work together with the column and alter its failure mode. Furthermore, they increased the column shear strength and decreased its capacity for deformation. However, the static performance of a single element cannot reveal the seismic behaviour of the entire structure. Therefore, some researchers have investigated the global behaviour of RC frames retrofitted by wing walls. Huang [17] conducted a series of quasi-static tests on a 2-storey, 2-bay nonductile frame with a weak



(a) Front view of the single span frame with severe



(b) Side view of the single span frame



(c) Internal damage of the classroom



(d) Crushed concrete at both ends of columns

Fig. 1. A sing-span RC frame damaged in Luding Ms 6.8 earthquake (2022) [5].

first storey retrofitted with wing walls. Klatakcı [18] conducted three static cyclic tests on 2-storey, 2-bay, and 1/3-scale specimens to investigate the experimental behaviour of vulnerable multistorey, multi-bay, and reinforced concrete frames retrofitted by wing walls under a lateral load. Kabeyasawa [19] presented the results of a static loading test on a full-scale five-storey reinforced concrete building using columns with wing walls.

Although the aforementioned quasi-static tests can yield the ultimate bearing capacity of RC frames with wing walls, they cannot reflect the dynamic effect during cyclic loading. Bai [20] carried out a series of pseudo-dynamic tests (PDTs) and quasi-static tests (QSTs) on a dual wing-walled frame system, which is a 1/7-scaled composite moment frame with steel-reinforced concrete (SRC) columns and reinforced concrete (RC) wing walls. Yang [6] investigated the seismic performance of an RC frame structure retrofitted with a wing wall using shaking-table tests on a 3-storey, 2-bay, 1/4-scale specimen. The shaking table test is a preferred method to account for dynamic effects [21]; however, these studies did not focus on single-span school buildings. In addition, in the absence of comparative tests, especially lack of shaking table tests on the same board ensuring the same excitation conditions, it is difficult to determine to what extent the effectiveness of wing wall-retrofitting frames can be achieved.

The scope and objective of this study are to compare the seismic performances of single-span RC frames with and without wing wall retrofitting, which were placed on the same board and loaded simultaneously using shaking table tests. The remainder of this paper is organised as follows. First, the process of determination of a retrofit scheme is introduced in Section 2. The structural model and test program are presented in Section 3. Finally, the test results and analyses are presented in Section 4, and the conclusions are summarised in Section 5.

2. Determination of retrofit scheme

In this section, the target structure is described, and the wing wall retrofitting scheme is determined based on a comparison of different retrofit schemes using numerical simulation.

2.1. Target structure

The target structure is a single-span reinforced concrete (RC) frame structure with a cantilevered corridor, which is a typical school building form in southern China [22], as shown in Fig. 2. There are four storeys in this structure, and the height of each storey is 3.6 m. On each floor, there are three identical classrooms. The structural details before retrofitting are presented in Fig. 2(b).

The design of the target structure was based on the Code for the Seismic Design of Buildings in China (GB50011-2001) [23]. The fortification intensity was VII (design acceleration was 0.15 g), and the site classification was Category II ($250 \text{ m/s} < V_{se} < 500 \text{ m/s}$). The column section measured 500×500 mm. The width of beam sections is 250 mm, and the heights are 600 mm, 500 mm and 400 mm, respectively. The floor slab thickness was 120 mm. C30 concrete was used for the columns, beams, and slabs of the frame structure. In addition to the self-weight of the structure, the additional dead load for each floor was 1.5 kN/m^2 , the equivalent floor distribution load of the infilled wall was 2.5 kN/m^2 , and the live load for each floor was 2.0 kN/m^2 .

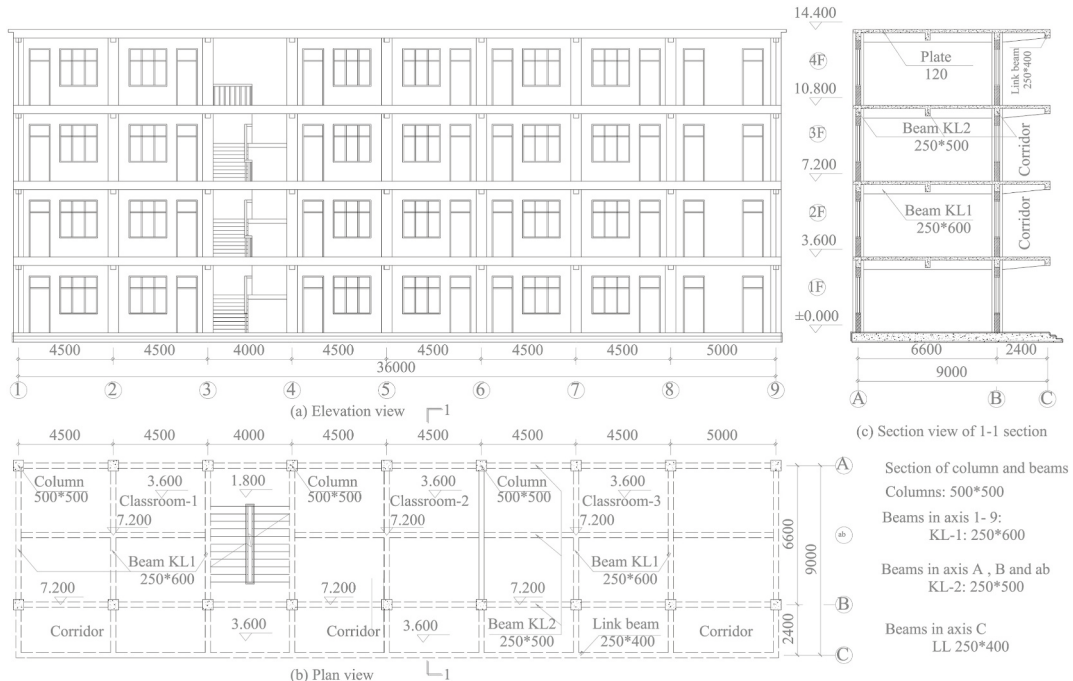


Fig. 2. A single-span RC frame structure with a cantilevered corridor.

2.2. Comparison of wing wall layouts

Retrofit schemes for unidirectional and bidirectional wing walls were adopted to strengthen the single-span school buildings, respectively. Unidirectional retrofitting involves the addition of wing walls in the Y direction, whereas bidirectional retrofitting involves the addition of wing walls in both the X- and Y-directions. Fig. 3 shows the layout of the wing wall retrofitting scheme, including combined sections of column and wing walls in one and two sides. The thickness of the wing walls was set to 200 mm, and the height of the wing wall cross sections changed from 300 mm to 700 mm, forming ten different retrofitting cases.

According to equal moments of inertia in the two directions and equal section area, an equivalent rectangular section can be obtained for each combined section of the column and wing walls. Equivalent section length-to-width ratio (ELWR) is defined as the length-to-width ratio of the equivalent rectangular section. The height of the wing wall sections and ELWR for different retrofit cases are listed in Table I and Table II. In the two tables, the retrofit case MHD refers to the different retrofit schemes, in which 'H' denotes the height of wing wall sections, and 'D' equates to 'u' or 'b', denoting unidirectional or bidirectional retrofit, respectively. I_{az} and I_{ay} denote the moment of inertia of the combined section.

According to Code for Design of Concrete Structures [24] and Technical specification for concrete structures of tall building [25], if the ELWR of the combined section is less than 4.0, the section should be designed in accordance with columns; otherwise, it should be designed according to walls. The ELWRs of the combined section in Table II with wing wall height $h_w \leq 600$ mm and those in Table I are less than 4.0. Therefore, the combined sections of column with wing wall in these cases can be treated as columns for modelling calculations. However, when the height of the wing wall is 700 mm in Table II, the ELWR of the combined section with wing wall on two sides was 4.373, which is greater than 4.0, and its mechanical performance is more like a wall rather than a column. Therefore, the cases M7b together with M7u was removed.

To find an optimal scheme for the single-span frame retrofit with a wing wall, nine numerical models, including one original frame (named M0) and eight retrofit cases, both unidirectional and bidirectional, were established using the MIDAS Software. In the models, the beam and column components, including the wing walls, were modelled using beam elements. The upper and lower ends of the wing walls are fixed to the beams, while the connection of wing walls to columns are neglected. Plastic hinges were used to simulate the elastoplastic properties of the members after yielding. The hinges on the beams adopted a tri-linear bending hinge, and the hinges on the columns adopted a PMM plastic hinge considering the coupling action of the axial force and bidirectional bending moments. For the definition of plastic hinge parameters, refer to the Midas user manual [26]. The mode-superposition response-spectrum method was employed to calculate the seismic responses in the nine cases. The fundamental periods and maximum lateral displacements on each floor in the nine cases were compared.

The fundamental periods in the X- and Y-directions for each retrofitting cases are listed in Table III. The first natural vibration period of the prototype structure is 0.6229 s in the X-direction and 0.6963 s in the Y-direction. For each unidirectional retrofit case using a wing wall, the fundamental period decreases in the Y-direction and increases in the X-direction. This is because the stiffness in X-direction hardly changed, but the mass increased after the addition of wing walls, and the period in the X-direction increased. It

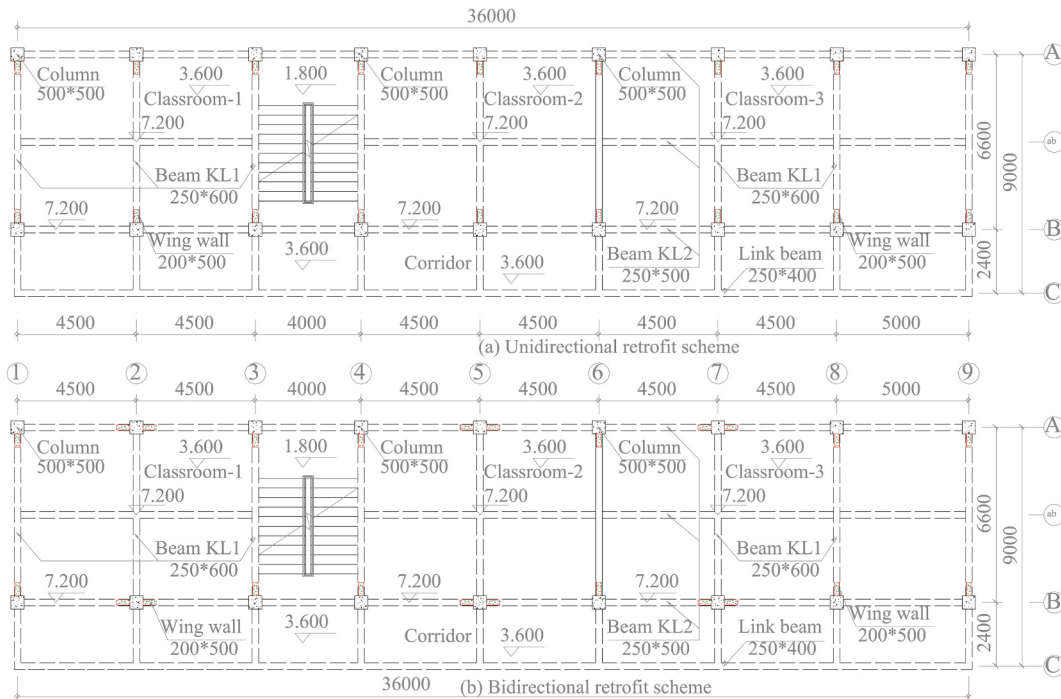


Fig. 3. Layout of wing wall retrofitting of the structure.

Table 1

ELWR of combined section of column with wing wall on one side.

Retrofit cases, MHD	M3u	M4u	M5u	M6u	M7u
Wall section height, h_w	300	400	500	600	700
Moment of inertia, I_{az}	1.34×10^{10}	1.85×10^{10}	2.51×10^{10}	3.33×10^{10}	4.32×10^{10}
Moment of inertia, I_{ay}	5.41×10^9	5.48×10^9	5.54×10^9	5.61×10^9	5.68×10^9
ELWR = $\sqrt{I_{az}/I_{ay}}$	1.574	1.841	2.130	2.438	2.760

Table 2

ELWR of combined section of column with wing walls on two sides.

Retrofit cases, MHD	M3b	M4b	M5b	M6b	M7b
Wall section height, h_w	300	400	500	600	700
Moment of inertia, I_{az}	2.53×10^{10}	3.97×10^{10}	5.94×10^{10}	8.50×10^{10}	1.17×10^{11}
Moment of inertia, I_{ay}	5.61×10^9	5.74×10^9	5.88×10^9	6.01×10^9	6.14×10^9
ELWR = $\sqrt{I_{az}/I_{ay}}$	2.124	2.631	3.179	3.761	4.373

Table 3

Fundamental periods of the structures in different retrofit cases (s).

Cases	Sec. height in X(mm)	Sec. height in Y(mm)	Period In X (s)	Amplitude of variation	Period in Y (s)	Amplitude of variation
M0	0	0	0.6229	0.00%	0.6963	0.00%
M3u	0	300	0.6327	1.57%	0.6271	-9.94%
M4u	0	400	0.6411	2.92%	0.6000	-13.83%
M5u	0	500	0.643	3.23%	0.5806	-16.62%
M6u	0	600	0.6521	4.69%	0.5826	-16.33%
M3b	300	300	0.5416	-13.05%	0.6302	-9.49%
M4b	400	400	0.5284	-15.17%	0.6025	-13.47%
M5b	500	500	0.51	-18.12%	0.5843	-16.09%
M6b	600	600	0.496	-20.37%	0.5871	-15.68%

demonstrates that when unidirectional wing wall retrofitting is adopted, the structure becomes stronger in the direction with wing walls, whereas it becomes weaker in the other direction. Consequently, a unidirectional retrofit scheme using a wing wall is unreasonable. For each bidirectional retrofit cases using wing walls, the fundamental periods of the structure in both directions decreased with an increase in the wing wall section height. The maximum reduction occurred in Case M6b, and the periods in the X- and Y-directions decreased by 20.37% and 15.68%, respectively.

The maximum lateral displacements of each floor for each retrofit cases under a design-based earthquake are presented in Table IV and Fig. 4. For all unidirectional retrofit cases using wing walls in Y-direction, the maximum lateral displacements decreased in the Y-direction, while they increased in X-direction. This further demonstrates that the unidirectional retrofitting scheme for adding wing walls in only one direction is unreasonable. For each bidirectional retrofit scheme using wing walls, the maximum lateral displacements of the structure in both directions decreased and became smaller with an increase in wing wall section height. The maximum reduction was in the case of M6b, where the maximum lateral displacements in the X and Y directions on the roof decreased by 32.93% and 19.21%, respectively [27].

2.3. Determination of wing wall retrofitting scheme

From the above seismic response analysis of each retrofitting cases using three-dimensional finite element, if the unidirectional wing walls are added in the single-span direction of the frame structure, the seismic response of the retrofitted structure will decrease in the single-span direction but increase in the other direction. If bidirectional retrofit schemes are adopted, the fundamental period

Table 4

Maximum floor displacements in X and Y direction (mm).

Case	Direction	1F	2F	3F	4F	Case	Direction	1F	2 F	3 F	4 F
M0	X	3.69	8.60	12.50	14.70	M0	X	3.69	8.60	12.50	14.70
	Y	4.39	10.71	15.92	19.10		Y	4.39	10.71	15.92	19.10
M3u	X	3.66	8.62	12.58	14.80	M3b	X	2.35	6.10	9.35	11.48
	Y	3.38	8.85	13.60	16.80		Y	3.40	8.93	13.77	16.99
M4u	X	3.95	9.23	13.40	15.80	M4b	X	2.06	5.53	8.68	10.90
	Y	2.92	7.94	12.50	15.70		Y	2.96	8.05	12.69	15.97
M5u	X	4.00	9.33	13.50	16.00	M5b	X	1.78	4.95	7.96	10.23
	Y	2.62	7.31	11.70	15.00		Y	2.67	7.44	11.95	15.27
M6u	X	4.17	9.65	13.90	16.40	M6b	X	1.59	4.54	7.48	9.86
	Y	2.66	7.38	11.82	15.10		Y	2.72	7.55	12.1	15.43

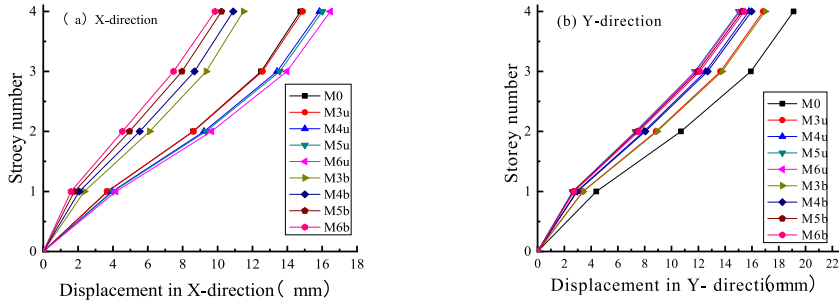


Fig. 4. Comparison of maximum displacement in each storey: (a) X-direction and (b) Y-direction.

and maximum lateral displacement of each cases will decrease compared with those of the original structure. It can be seen that for the single-span frame structure, the bidirectional retrofit scheme with wing walls should be adopted. In other words, the wing walls should be arranged in both directions, so that the seismic capacity can be improved in both directions.

To study the seismic capacity of the single-span frame retrofitted with wing walls, a nonlinear static (pushover) analysis of the original structure, M0 and M3b to M6b of the bidirectional wing wall retrofit cases, was performed using MIDAS software. The lateral load adopt an inverted triangle (first mode) load pattern, and the target displacement was set as the 2% total height of the frame. The capability curves of the single-span frame retrofitted with wing walls are shown in Fig. 5. The structural performance points of the M3b–M6b cases under the action of rare earthquake (2% exceedance probability in 50 years) are listed in Table V.

As can be seen from Fig. 5(a), the seismic capacity in the X-direction for the four schemes is clearly higher than that of the original structure, and the ductility does not change significantly, whereas the seismic capacity of each retrofit scheme is almost similar. From Fig. 5(b), it can be seen that the seismic capacity in the Y-direction of the retrofitted structure is greatly improved, whereas the deformation capacity of the structure decreases with an increase in the length of the wing wall, but the decrease is not significant. The sudden drops in base shear forces vs. roof displacement, particularly for M3b in X-direction and M6b and M5b in Y-direction are because some plastic hinges in the wing wall and beam ends have reached the ultimate bearing capacity point in the skeleton curve, numerical iterations did not converge after the models continued to be loaded. As shown in Table V, performance points can be obtained by intersecting the capability spectra of the structures and the seismic demand spectra of the maximum considered earthquakes in the X- and Y- directions of these four schemes, indicating that the deformation of these four schemes in the two directions meets the elastic-plastic deformation requirements of the maximum considered earthquakes. Through pushover analysis, it was found that the seismic capacity of the structure improved for the four retrofit schemes, and with an increase in the wing wall length, the seismic capacity became stronger. Compared with the original structure, although some of the deformation capacity decreases, it still meets the requirements of elastic-plastic deformation under rare earthquakes. Among these four cases, M5b and M6b had better retrofit effects in terms of improving the load-carrying capacity.

From a construction perspective, the calculated span of the frame beam will be shortened after adding the wing wall, and the length required by the negative reinforcement bars of the support will be reduced accordingly. When the size of the wing wall is relatively large, the negative bending moment bearing capacity of the frame beam support should be checked. It is assumed that if the height of the wing wall section is not greater than $L_n/12$ (L_n denotes the span of the beams), the negative reinforcement bars after retrofitting can be guaranteed to be no less than 10% of the required amount; otherwise, the amount of retrofit engineering will be relatively large. The span of this prototype structure is 6600 mm; therefore, the height of the wing wall section should not exceed $6600/12 = 550$ mm. Based on the above structural analysis and construction guidelines, it was concluded that a bidirectional retrofit scheme with a wing wall section height of 500 mm was the most appropriate retrofit scheme for this structure.

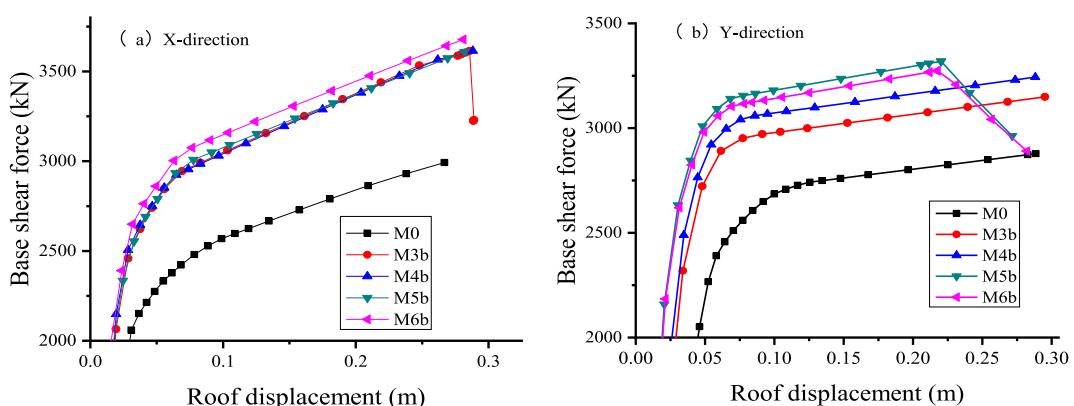


Fig. 5. Base shear force vs. roof lateral displacement in (a) X-direction and (b) Y-direction.

Table 5
Performance points of the structure with different retrofit schemes under earthquake.

	Case	Spectral acceleration	Spectral Displacement	Base shear force (kN)	Roof displacement (mm)	Effective damping ratio (%)	Effective Period (s)
X dir	M3b	0.2618	0.07751	3051	100.60	22.13	1.092
	M4b	0.2826	0.07126	3005	88.80	21.87	1.007
	M5b	0.273	0.08016	2933	64.20	19.78	1.087
	M6b	0.2734	0.07959	2987	61.60	19.93	1.083
Y dir.	M3b	0.2374	0.0892	2991	110.80	21.54	1.230
	M4b	0.246	0.0867	3069	104.10	21.12	1.191
	M5b	0.2498	0.0825	3173	95.25	21.98	1.153
	M6b	0.2458	0.0837	3136	96.35	22.12	1.171

3. Structural model and test program

In order to compare the seismic behaviour of the single-span RC frame without and with wing wall retrofit, the classrooms in A-C/① -③ in Figs. 2(b) and 3(b) were selected as the prototype structures, respectively. The corresponding information of the prototype structure is listed in Table VI. First, the similitude law for the structural models was determined. Second, the design details of the two specimens—the single-span RC frame and an identical frame with a wing wall retrofit—are presented. The test setup and instrumentation are also illustrated. Finally, the input ground motions and test sequences are described.

3.1. Similitude law

To make full use of the size and payload capacity of the shaking table facility, the models were designed to a 1:5 scale, that is, the length ratio S_L is 0.2. The 1:5 scale models were fabricated using micro concrete. Based on experience, the elastic modulus ratio between the micro concrete and prototype concrete S_E was assumed to be 1:1.6, to design an artificial mass before the tests.

An important parameter in defining the similitude law is the amount of artificial mass to be added to the model [28,29]. The mass-scale factor obtained from the ideal similitude law is expressed as follows:

$$\frac{(m_m)_{\text{total}}}{(m_p)_{\text{total}}} = \frac{m_{\text{ms}} + m_{\text{ma}}}{m_{\text{ps}} + m_{\text{pn}}} = S_E S_L^2, \quad (1)$$

where $(m_m)_{\text{total}}$ = total mass of the model (including model self-weight m_{ms} and artificial mass m_{ma}), and $(m_p)_{\text{total}}$ = total mass of the prototype building (including structural self-weight m_{ps} , additional dead load, nonstructural components, and live load m_{pn}).

The total mass of the prototype structure without wing wall retrofit was $(m_p)_{\text{total}} = 385$ t, including the structural self-weight $m_{\text{ps}} = 190$ t and the mass derived from the non-structure (infilled wall) and live load $m_{\text{pn}} = 194$ t. The total mass of the prototype structure with the wing wall retrofit was 394 t, including a structural self-weight of 200 t. As the mass of the latter was very close to that of the former, the artificial masses of the two models (specimens) were calculated according to the mass of the prototype structure without a wing wall retrofit. The model self-weight m_{ms} can be determined by

$$m_{\text{ms}} = m_{\text{ps}} \cdot S_p S_L^3, \quad (2)$$

where S_p is the mass-density ratio. Since the density of prototype concrete is 2400 kg/m³, and the density of micro-concrete is 2300 kg/m³, S_p is equal to 0.96.

According to Eq. (2), the self-weight of one model (specimen) is 1.5 t. Using Eq. (1), the artificial mass added to each model is calculated as 8.1 t. After the mechanical property test of the micro concrete, it was found that the actual elastic modulus ratio, S_E was 1/2.2. The equivalent mass density ratio can be obtained using Eq. (3), and the result is 3.125.

$$\bar{S}_p = \frac{m_{\text{ms}} + m_{\text{ma}}}{S_L^3 \times (m_p)_{\text{total}}} \quad (3)$$

Because the equivalent mass density ratio is not equal to S_E/S_L , the scale factors for time, frequency, and acceleration can be adjusted according to Eq. (4)- Eq. (6).

Time ratio:

$$S_t = S_L \sqrt{\bar{S}_p / S_E} \quad (4)$$

Frequency ratio:

$$S_\omega = \sqrt{S_E / \bar{S}_p} / S_L \quad (5)$$

Acceleration ratio:

$$S_a = S_E / (S_L \bar{S}_p) \quad (6)$$

The similarity constants and ratios include four main aspects: geometry, material, load, and dynamics, which are listed in Table VII.

Table 6

Information of prototype and model structures.

Item	Prototype	1/5 model
Storey height	3.6 m	0.72 m
Total height	14.4 m	2.88 m
Plan dimension	9 m × 9 m	1.8 m × 1.8 m
Section of beams	250 mm × 600 mm 250 mm × 500 mm 250 mm × 400 mm	50 mm × 120 mm 50 mm × 100 mm Ignored
Section of columns	500 mm × 500 mm	100 mm × 100 mm
Thickness of plate	120 mm	24 mm
Material	C30	micro-concrete C10

3.2. Specimen design details

Two specimens were constructed based on the similarity relationships derived above. The one with wing walls retrofit was denoted as Model-A, and the other without wing walls retrofit was denoted as Model-B. The plan, elevation, and side views of specimens A and B are shown in Figs. 6–9. The link beam on axis C of the prototype structure (Fig. 2) was ignored in the two specimens. In addition, cantilever beams of variable cross-sections in the prototype structure were constructed as a constant cross-section in the two specimens.

The materials used for the specimen were micro concrete C10 and a zinc-coated wire. For the columns, #8 wire was used as the longitudinal bar, and #14 wire was adopted as the stirrup. For the reinforcement of the beams, #4 and #8 steel wires were used as the beam longitudinal bars, and #14 wire was used for the stirrups. A #10 wire was used for the slab reinforcement. Wires #10 and #14 were used as the longitudinal and transverse bars of the wing walls, respectively. The test results for the mechanical properties of micro concrete and wires are presented in Table VIII and Table IX, respectively.

For Model-A, the model size is so small that if the drilling of holes and planting a steel bars in the column and beam of the specimen were implemented after construction, the specimen would be damaged. Furthermore, because there was no notch on the surface of the wire, the anchor of the wire would not be sufficiently firm if planted. In this test, some of the wing wall wires were pre-buried in the columns and beams of Model-A. Following the construction of the main structure (columns, beams, and slab) of the specimen, the vertical reinforcement of the wing wall were installed and welded to the pre-buried wires in the beams. The pre-buried wires in the column were bended, forming the horizontal reinforcement of the wing wall. The templates were then set up, and the micro concrete of the wing walls was cast. The column and wing wall reinforcements are shown in Figs. 10 and 11.

3.3. Test setup and instrumentation

The tests were conducted at the earthquake simulation facility of the Institute of Engineering Mechanics, China Earthquake Administration. The facility consists of a 5 m × 5 m steel platform with six degrees of freedom, driven by servo-hydraulic actuators, and an electronic control system that provides robust feedback of acceleration, velocity, and displacement. The payload capacity of the shaking table is approximately 30 t, and its maximum horizontal acceleration is 1.0 g. The data acquisition system is capable of sampling up to 128 channels at a rate of 100 samples/s for each channel.

The two specimens were placed on the same table and simultaneously tested, see Fig. 12. As noted above, the one retrofitted the wing wall retrofit is denoted as A (on the left in Fig. 12), and the one without retrofitting is denoted as B (on the right in Fig. 12) [30].

The global and local behaviours of the specimens and the motion of the shaking table were monitored using an instrumentation network of accelerometers and displacement transducers. There were nine displacement transducers (DT1–DT9) and nine accelerometers (AM1–AM9) in total. They were used to monitor the displacement and acceleration of the two specimens in the Y-direction. The layouts of the instruments are shown in Figs. 6 and 13. For Model-A, a displacement transducer and an accelerometer were installed at points A and B, respectively, on each floor. For Model-B, a displacement transducer and accelerometer were installed at point D on each floor. Another accelerometer was placed on the shaking table at point C.

According to the characteristics of seismic damage to frame structures, the inter-storey drifts of the bottom floors were much larger than those of the top floors. However, the displacement responses of the bottom floors were not evident under a small seismic excitation. To obtain ideal inter-storey drift responses, several tensile displacement transducers were placed along the diagonal directions of the first and second floors. This arrangement is shown in Fig. 13.

3.4. Ground motions and test sequence

The input ground motion consisted of three accelerations and was applied parallel to the single-span y-axis). These are the ground motion records of EL Centro, Taft, and Wolong, which were selected according to the standard design response spectrum. The acceleration time histories and spectra of the three ground motions are shown in Fig. 14. According to the similarity relation of time, the scaling factor for the input ground motion duration was approximately 0.5.

The test program also included low-intensity white noise excitation between the earthquake tests. Based on the Code of Seismic Design of Buildings in China (GB50011-2010) and the similarity relationship, the input PGA was adjusted to simulate the seismic response under different seismic intensities. The natural vibration frequency measured with white noise vibrations was used for system and damage identification before and after every earthquake test to establish the degree of damage after each input motion. The test

Table 7
Similarity relation.

Physical parameter	Symbol	Initial similitude law	Updated similitude law	Remark
Length ratio	S_L	1/5	1/5	Control dimension
Elasticity modulus ratio	S_E	1/1.6 ⁽¹⁾	1/2.2 ⁽²⁾	Control material
Stress ratio	$S_\sigma = S_E$	1/1.6	1/2.2	
Equivalent density ratio	\bar{S}_ρ	3.125	3.125	Eq. (3)
Time or Period ratio	$S_t = S_L \sqrt{\bar{S}_\rho / S_E}$	1/2.2	1/1.9	Eq. (4)
Frequency ratio	$S_\omega = \sqrt{S_E / \bar{S}_\rho} / S_L$	2.2	1.9	Eq. (5)
Acceleration ratio	$S_a = S_E / (S_L \bar{S}_\rho)$	1	1/1.37	Eq. (6)

Note: (1) The elastic modulus ratio of 1/1.6 in the initial similitude law was determined based on experience before shaking table test. (2) The elasticity modulus ratio of 1/2.2 in the update similitude law was determined according to the mechanical property test of the micro-concrete.

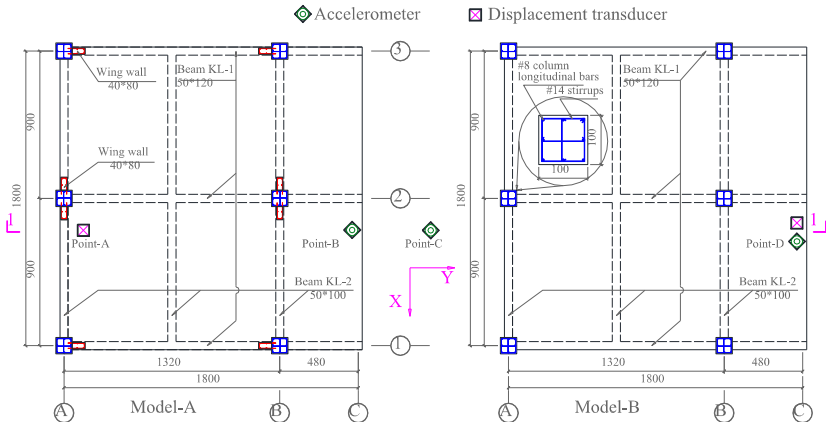


Fig. 6. Plan view of Model-A and B with instrument layout (unit: mm).

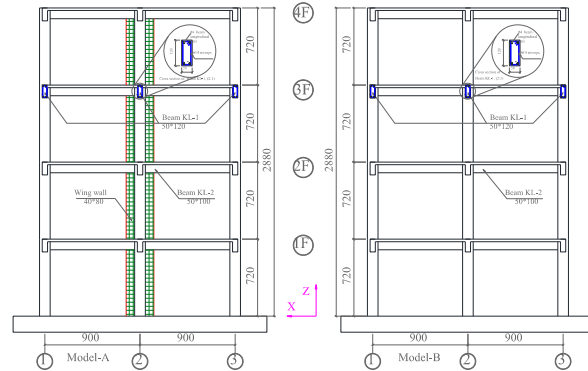


Fig. 7. Elevation view of Model-A and B.

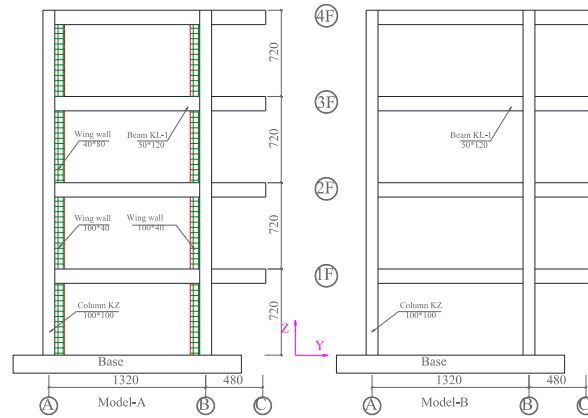


Fig. 8. Side view of Model-A and B (unit: mm).

sequences used in the experiments are listed in [Table X](#).

4. Test results and analyses

This section describes the observed experimental phenomena of the two specimens. The measured experimental results are presented and analysed.

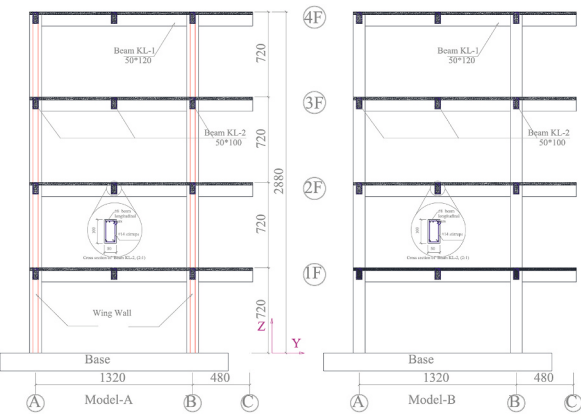


Fig. 9. Section view of Model-A and B in 1-1 section with instrument layout (unit: mm).

Table 8
Mechanical properties of micro concrete.

Floor number	Elasticity modulus (MPa)	Compressive strength (MPa)
1	1.4284×10^4	11.89
2	1.3555×10^4	12.51
3	1.3001×10^4	11.94
4	1.3701×10^4	12.00
mean	1.3613×10^4	12.08

Note: (1)compressive strength was obtained through the concrete cube test; (1)elasticity modulus was obtained through the concrete prism test.

Table 9
Mechanical properties of the reinforcements (wires).

Type	Diameter (mm)	Elastic modulus (GPa)	Yield stress (N/mm ²)	Ultimate stress (N/mm ²)	Elongation rate
#4	5.893	215.6	254	382	0.13
#8	4.064	208.5	270	385	0.15
#10	3.251	203.8	301	390	0.17
#14	2.032	196.4	337	409	0.17

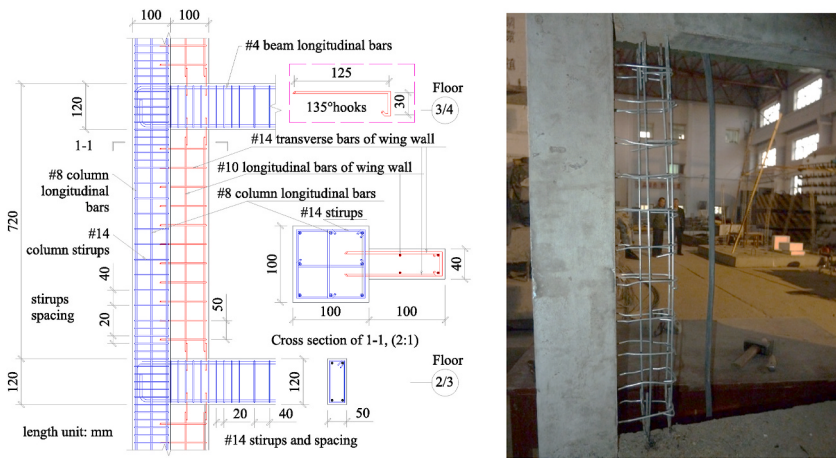


Fig. 10. Structural details and reinforcement of the column with one side wing walls (Axis A).

4.1. Observed experimental phenomena and analysis

The development of cracks in the two specimens with increasing ground-motion intensity is described. According to Classification of earthquake damage to buildings and special structures [31], Five damage states [4,32], named none, minor, moderate, severe and

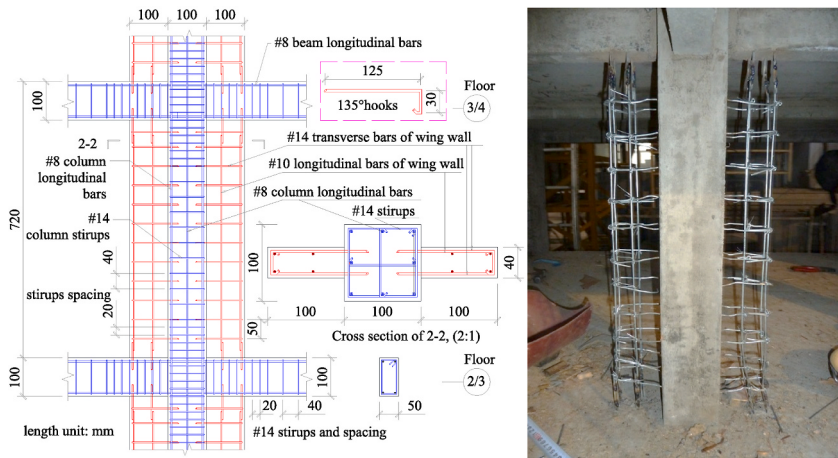


Fig. 11. Structural details and reinforcement of column with two side wing walls (Axis-②).

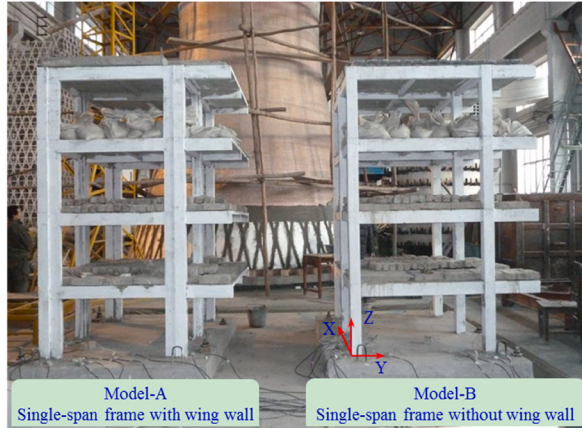


Fig. 12. Two specimens on the shaking table.

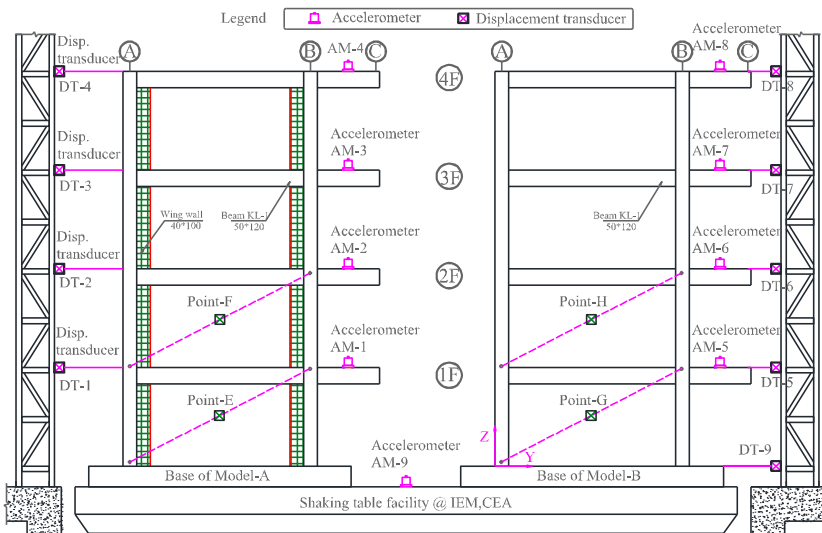


Fig. 13. Side view of Model-A and B with instrument layout.

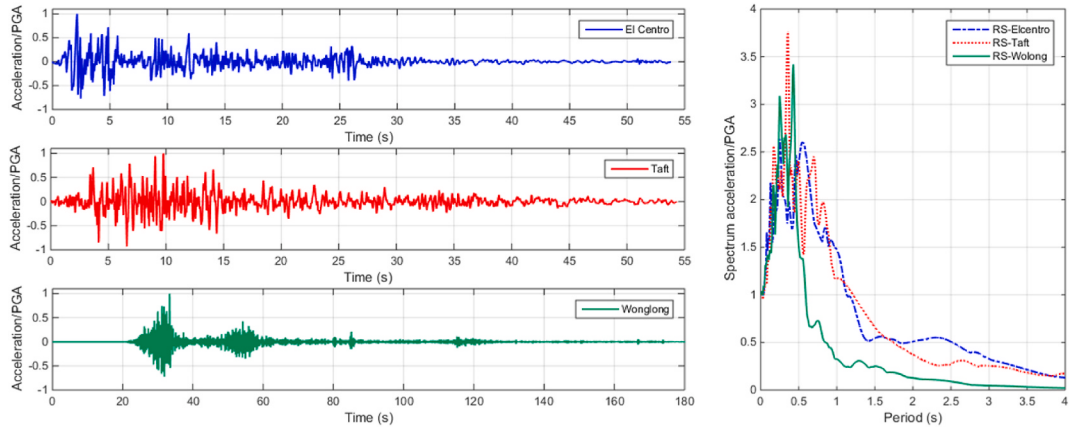


Fig. 14. The input acceleration time histories and spectra of the ground motion records.

Table 10
Test sequence at each intensity level.

Load case	Earthquake records	PGA in plan	PGA in practical	remark
1	White noise	0.02 g	0.02 g	first
2	El Centro	0.05 g	0.07 g	–
3	Taft	0.05 g	0.05 g	–
4	Wolong	0.05 g	0.05 g	–
5	White noise	0.02 g	0.02 g	second
6	El Centro	0.15 g	0.12 g	–
7	Taft	0.15 g	0.12 g	–
8	Wolong	0.15 g	0.11 g	–
9	White noise	0.02 g	0.02 g	third
10	El Centro	0.20 g	0.25 g	–
11	Taft	0.20 g	0.20 g	–
12	Wolong	0.20 g	0.20 g	–
13	White noise	0.02 g	0.02 g	fourth
14	El Centro	0.30 g	0.35 g	–
15	Taft	0.30 g	0.30 g	–
16	Wolong	0.30 g	0.30 g	–
17	White noise	0.02 g	0.02 g	fifth
18	El Centro	0.40 g	0.42 g	–
19	Taft	0.40 g	0.40 g	–
20	White noise	0.02 g	0.02 g	sixth

collapse, under different cases are determined by the test phenomena. In addition, the corresponding maximum Inter-storey drift ratios (IDR) in average $\bar{\theta}_m$ are also offered.

No visible cracks could be found on the two specimens when the PGA of excitation was smaller than 0.05 g. With the input PGA of 0.15 g, clear cracks were first observed in Model-B, whose cracks were first formed at the beam ends and the top ends of corner columns. Its damage state was moderate, and maximum IDR in average $\bar{\theta}_m$ was 1/124. However, the columns of Model-A remained intact, and only a few tiny cracks appeared in the construction joints between the wing walls and the beam on the second and third floors. Its damage state was minor with $\bar{\theta}_m$ equal to 1/244.

When the target PGA of the excitation reached 0.20 g, both specimens exhibited a fierce dynamic response. It is worth mentioning that the measured acceleration on the shaking table board was 0.25 g for the El Centro case. For Model-B, the cracks at the beam ends of the first and second floors widened, meanwhile tiny cracks started to occur at the beam ends on the third floor. The cracks at the top ends of the corner columns began to propagate outwards, and tiny cracks formed at the top ends of the middle and corner columns on the second floor. The damage state of Model-B was moderate with $\bar{\theta}_m$ equal to 1/75. In contrast, the columns in Model-A remained in a good state, except that the cracks in the middle of the beams on the third floor developed towards the beam centre. Cracks were formed along the construction joints of the beam and wing wall, and moderate damage occurred to Model-A with $\bar{\theta}_m$ equal to 1/129.

After the PGA of the excitation reached 0.30 g, Model-B suffered permanent/sustained damage. Vertical cracks at the beam end penetrated the joints on the second floor. The cracks at the bottom of the beam on the third floor widened and developed diagonally, see Fig. 15. In addition, cracks at the top end of the column on the third floor penetrated the joints with a small amount of spalling concrete, as shown in Fig. 16. The damage of Model-B was severe with $\bar{\theta}_m$ equal to 1/47. In contrast, for Model-A, a large number of cracks appeared in the beam-wing wall joints and developed towards the middle of the beams, and the side columns were slightly damaged, with a few tiny cracks, as shown in Figs. 17 and 18. The damage of Model-A was moderate with $\bar{\theta}_m$ equal to 1/69.

When the PGA of El Centro and Taft were equal to 0.40 g, the damage of Model-B became critical. The beams on the first and second floors suffered serious damage, and penetrating cracks appeared at most of the beam ends, as shown in Figs. 19 and 20. The concrete was crushed at the top ends of the side columns on the first and second floors and the middle columns on the second and third floors. Model-B was in collapse damage state with $\bar{\theta}_m$ reached 1/26. In contrast, many cracks in Model-A propagated from the beam ends to the mid-span and were evenly distributed, as shown in Fig. 21. Obvious destruction on the construction joints between beam and wing walls can be observed, as is seen in Fig. 22. Model-A was in severe damage state, and $\bar{\theta}_m$ reached 1/49.

Following the destruction phenomenon, the most severely damaged part of Model-B was on the second floor. After an input acceleration of 0.30 g, plastic hinges were formed on the beam ends owing to penetrating cracks, and wide cracks appeared in the bottom part of the mid-beam and propagated diagonally. At the top end of the side column on the second floor, the concrete was crushed, and plastic hinges took shape. When the input acceleration reached 0.40 g, cracks on the beam ends of the first and second floors propagated rapidly and contributed to the formation of plastic hinges. The concrete at the top ends of the side columns of the first and second floors, and that on one of the mid-columns on the third floor were crushed, and plastic hinges were formed. The overall damage to Model-B is illustrated in Fig. 23. The seismic capacity was estimated to be the ultimate value under such circumstances. By comparison, the most severely damaged part of Model-A was on the third floor. When subjected to an input acceleration of 0.30 g, cracks in the beam ends propagated towards the middle part of the beams, and the joints of the wing walls and beams were also damaged, as indicated by the cracks that appeared in those joints. When the input acceleration reached 0.40 g, the cracks propagated rapidly and were evenly distributed on the beams, and the diagonal cracks in the joints of the wing wall and beams became wider, as did the cracks on the columns, as shown in Fig. 24. The average maximum IDR of Model-A reached 1/49, and the seismic performance level was in severe damage state.

In Model-B, all vertical cracks in the beam end rapidly widened owing to the continuous dynamic loading, resulting in the formation of plastic hinges, which indicated a shortage of energy-dissipation capacity. The spalling concrete at the top ends of the columns indicated that plastic hinges formed; for instance, after an input acceleration of 0.40 g, a few plastic hinges took shape at the column ends. Because the redundancy of single-span RC frames is relatively low, only a few plastic hinges may have a critical impact on the structure and trigger a transformation from a statically indeterminate structure to a mechanism which may cause a total progressive collapse owing to the domino effect. From the perspective of overall deformation, it is assumed that the collapse may occur when maximum IDR of the RC frame reaches 1/25. In comparison, cracks were also observed in Model-A. However, because of the existence of wing walls, cracks in the beams were evenly distributed, and they were not concentrated at specific spots. Consequently, the energy dissipation capacities of these components were higher than those of Model-B.

4.2. Measured experimental results and analyses

In this subsection, the measured experimental results, including the modal frequency, displacement, and acceleration responses, are presented and analysed.

4.2.1. Comparison of dynamic properties between the two specimens

The natural frequencies of the vibrations, measured with white noise excitation, were used for system and damage identification before and after each earthquake excitation. The results are listed in Table XI.

Fig. 25 shows a comparison of the first three frequencies for the two specimens during the deterioration process owing to increasing excitation intensity. Specifically, Fig. 25(b)–(d) illustrate the attenuation ratio between the i -th frequency $f_i(i)$ and the corresponding initial frequency $f_j(1)$, where j is the modal order, and i denotes the test ID of the white noise excitation. Fig. 25(a) shows that the frequency attenuation of the higher order mode owing to damage is more apparent than that of the first-order frequency.

The results presented in Fig. 25 and Table XI can also be used to reveal the damage processes in the two specimens.

- (1) The first white noise excitation showed that the first frequency and period of Model-B were $f_{B1} = 1.832$ Hz and $T_{B1} = 0.5458$ s, while the first frequency and period of Model-A were $f_{A1} = 2.653$ Hz and $T_{A1} = 0.3769$ s. The first frequencies or periods of the two specimens clearly indicate that the stiffness of Model-A is twice larger than that of Model-B.



(a) Location at axis- A/② on 2nd floor (b) Location at axis- B/② on 3rd floor

Fig. 15. Cracks at the beam ends of the 2nd and 3rd storeys of the frame without retrofitting.

(a) Location at axis B/Ø on 2nd floor (b) Location at axis B/Ø on 2nd floor

Fig. 16. Spalling of concrete at the column top on the 2nd floor of the frame without retrofitting.

(a) Location at axis A-B/Ø on 2nd floor (b) Location at axis A/Ø on 3rd floor

Fig. 17. Cracks on the beam and its ends on 2nd and 3rd floors of the frame with retrofitting.

(a) Location at axis A/Ø on 2nd floor (b) Location at axis B/Ø on 3rd floor

Fig. 18. Cracks in the side column ends on 2nd and 3rd floors of the frame with retrofitting.

- (2) From the results of the second white noise excitation, it can be seen that the first three frequencies of Model-B all started to decrease, and the first frequency decreased by approximately 5% to 1.744 Hz (95.2% f_{B1}). In contrast, the first three frequencies of Model-A were unchanged, which indicates that after the PGA of excitation reached 0.05 g, Model-A stayed elastic while Model-B was slightly damaged.
- (3) The results of the third white noise excitation showed that the frequencies of Model-A began to decrease, and its first frequency decreased by approximately 14% to 2.274 Hz (86% f_{A1}). However, the frequencies of Model-B decreased more rapidly than those of Model-A, and its first frequency decreased by approximately 22% to 1.349 Hz (73.6% f_{B1}), which indicates that model-B was damaged more severely at this stage (PGA of excitation was 0.15 g).
- (4) The results of the fourth white-noise excitation indicated that the frequencies of the two specimens continued to decrease. The first frequency of model-A decreased by 23% to 1.654 Hz (62.3% f_{A1}). By contrast, the first frequency of model-B decreased by 11% to 1.146 Hz (62.5% f_{B1}). This indicates that Model A was damaged more severely when the PGA of the excitation reached 0.20 g. Because there were construction joints between the wing wall and the bare frame, cyclic dynamic effects could easily cause disconnections in the construction joint spots. Therefore, the structural stiffness decreases rapidly. For Model-B, it has



(a) Joints at axis- A/① on 1st floor (b) Joints at axis- A/③ on 1st floor

Fig. 19. Destruction in the joints and beam-ends of Model-B.



(a) Joints at axis- A/① on 2nd floor (b) Joints at axis- A/③ on 2nd floor

Fig. 20. Penetrating cracks on the beam-ends of Model-B.



Fig. 21. Evenly distributed cracks on Model-A.



Fig. 22. Severe destruction on the connection between beam and wing wall of Model-A.

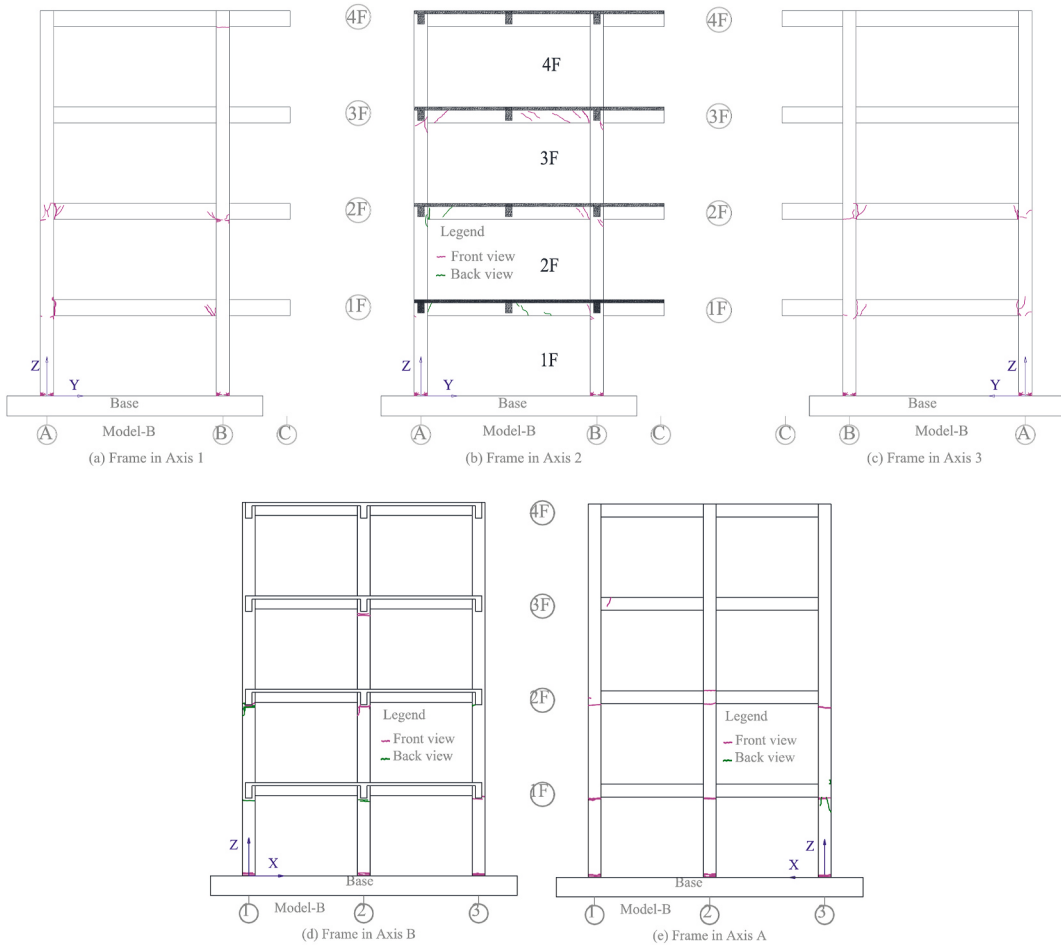


Fig. 23. Cracks after the final test for the frame without retrofit.

suffered a large damage in the last stage ($PGA = 0.15$ g), and its stiffness has degenerated to 53.3% of the initial stiffness. In addition, its fundamental frequency has moved away from the peak region of the response spectra input ground motions. As a result, the damages of model-B are not consistent with increasing PGA of 0.2 g.

- (5) The results of the fifth white noise excitation after the input ground motion 0.30 g show that the frequencies of the two specimens continued to decrease, and the decay rates of the frequencies for the two models were almost the same. At the end of the test, the first frequency decreased by 49% in total to 1.35 Hz for Model-A and decreased by 51% in total to 0.90 Hz for Model-B. It was also observed that the frequency of Model-A decreased significantly, whereas that of Model-B decreased only by a small value, especially the third frequency. Model-B reached its ultimate loading state. In contrast, redundancy remained in Model-A.

4.2.2. Comparison of displacement responses of the two specimens

The displacement responses of both specimens were measured using a displacement transducer on each floor. The peak floor displacement (PFD) responses under three ground motion excitations, El Centro, Taft, and Wolong, during different earthquake intensities, are illustrated in Figs. 26–28. Fig. 29 clearly shows the PFDs of each storey in another form for the two specimens under three ground motion excitations.

From Figs. 26–29, it can be seen that the peak floor displacements increased with the excitation. Compared with the PFD of the frame without retrofit, the corresponding PFD of the retrofitted frame decrease by 30%–40% when subjected to the same excitation intensity. Note that although the models were subjected to the same excitation intensity, the increase in the amplitudes of the two specimens was different. For example, the slope of the PFD vs. PGA curve for Model-A at $PGA = 0.40$ g becomes gradual, which means that the increase in PFD is small. By comparison, the slope of the PFD vs. PGA curve for Model-B at $PGA = 0.40$ g becomes steep, which indicates that the increase in PFD is large and dramatic. This can also be seen from Fig. 29.

Inter-storey drift ratio (IDR) is defined as the relative drift between two consecutive storeys normalised by storey height. This ratio is an important demand parameter that best correlates with the damage to the building. In this study, the IDRs for four floors were calculated based on the measured displacement responses. In addition, the IDRs of the bottom two floors were modified using the

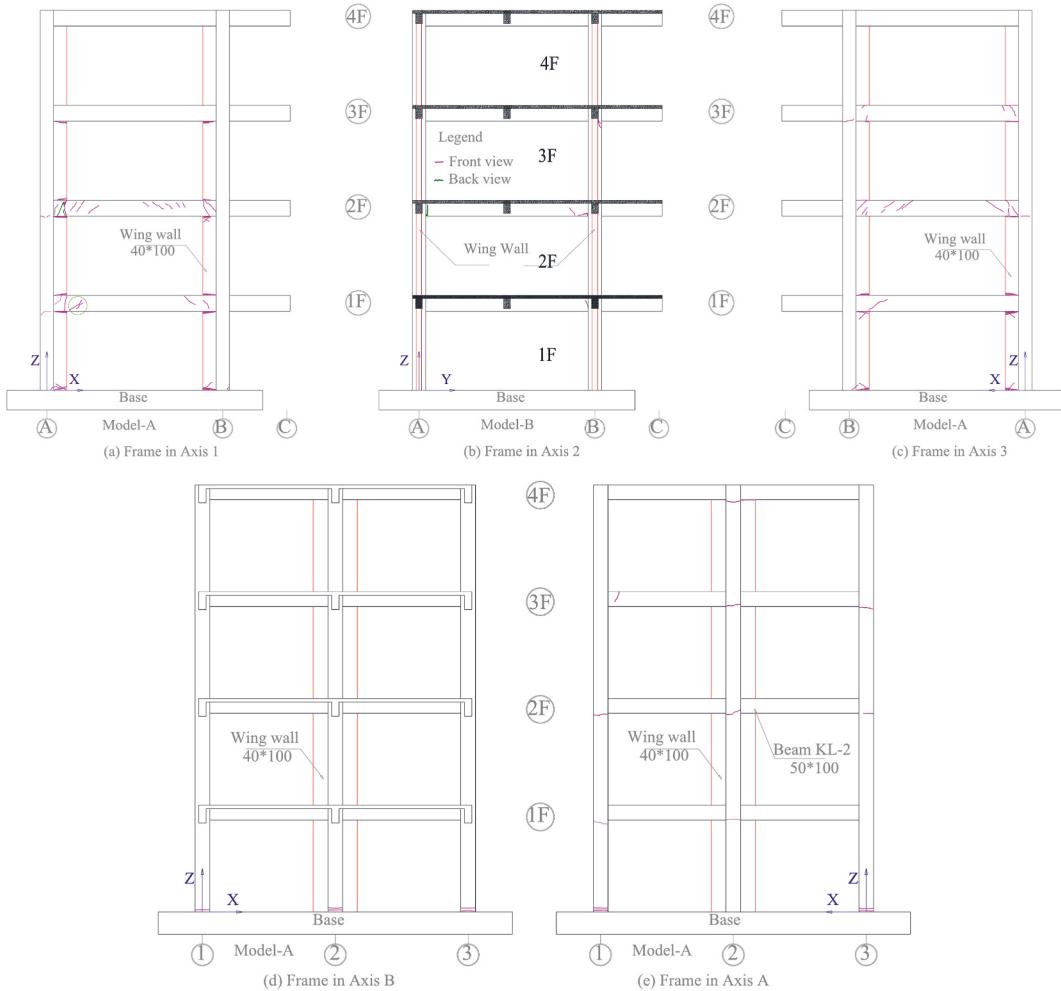


Fig. 24. Cracks after the final test for the frame with retrofit.

Table 11
Natural frequencies of the two specimens.

White noise sequence	Model-A			Model-B		
	1st Freq. (Hz)	2nd Freq. (Hz)	3rd Freq. (Hz)	1st Freq. (Hz)	2nd Freq. (Hz)	3rd Freq. (Hz)
1st	2.653	9.637	17.6	1.832	7.137	12.61
2nd	2.653	9.637	17.6	1.744	6.942	12.41
3rd	2.274	8.473	16.48	1.349	5.931	11.56
4th	1.654	6.604	13.35	1.146	4.989	9.913
5th	1.407	5.915	12.47	0.9268	4.359	8.741
6th	1.353	4.96	10.99	0.9017	4.007	8.679

results from the displacement transducers placed along the direction of the diagonal of the first and second floors. The IDRs of each floor during each loading case are listed in Table XII and illustrated in Fig. 30.

It can be seen from the maximum inter-storey drifts of the two specimens illustrated in Table XII and Fig. 30: (1) When subjected to the same level of ground motion, namely El Centro, Taft, and Wolong, the floor response of Model-B was evidently larger than that of Model-A, which revealed that the stiffness of the structure without retrofitting was weaker than that of the retrofitted structure. (2) The maximum IDR of the specimen without a retrofit appears on the second floor, whereas for the one with a retrofit, it mainly occurs on the third floor, and the IDR for the first to third floors are approximately the same. (3) For the two specimens, the IDR under the El Centro excitation is the largest, while those under the Taft and Wolong excitations are smaller.

(4) On average, the maximum IDR of the specimen without retrofitting reached 1/47 (exceeded 1/50) when the seismic excitation is 0.30 g, while that of the specimen with retrofitting reaches only 1/49 when the seismic excitation is 0.40 g, as shown in Fig. 30(g)-

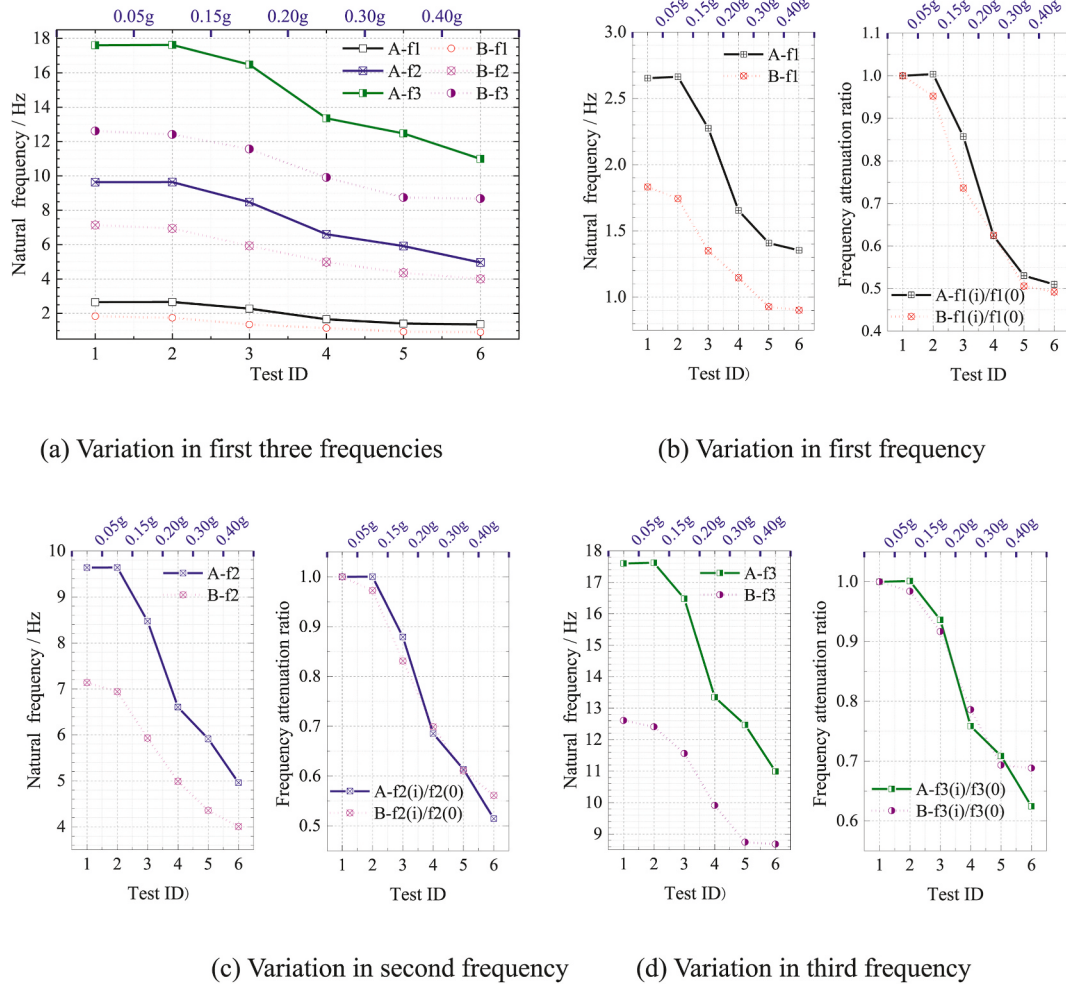


Fig. 25. Decrease in frequency with increase in excitation.

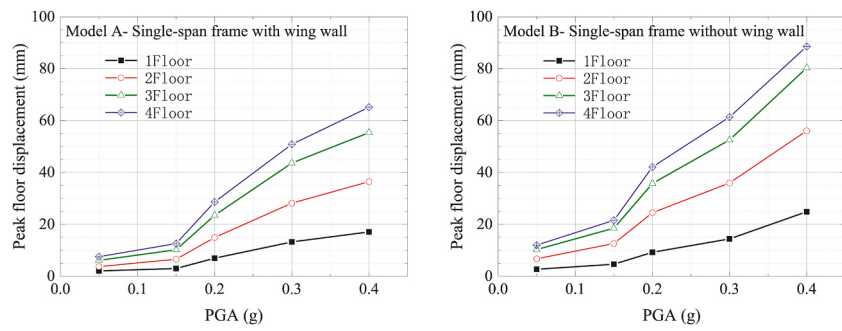


Fig. 26. Peak floor displacements versus PGA under El Centro excitation.

(h).

According to maximum IDR in average of the two specimens, damage states of the specimens under frequent earthquake, design based earthquake and rare earthquake are classified based on the standard in [Table XIII](#). The damage states of the two specimens are listed in [Table XIV](#).

As shown in [Table XIV](#), seismic performance of the single-span frame was improved by adding wing wall to the frame. When input PGA was 0.05g (frequent earthquake), the maximum IDR in average was 1/503, and none damage occurred to model-A. While the maximum IDR in average of Model-B was 1/330, which indicates it was in minor damage state. When input PGA was 0.15g (design

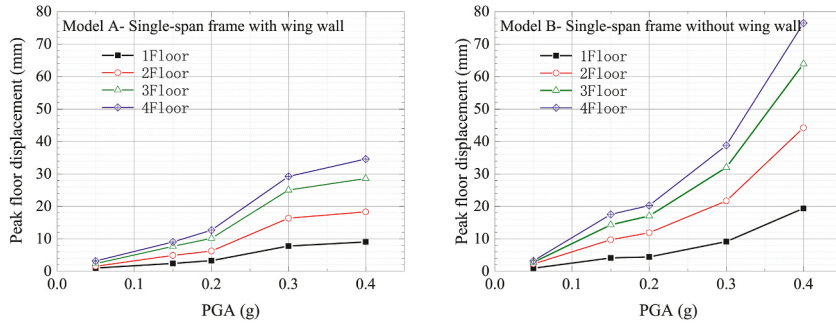


Fig. 27. Peak floor displacements versus PGA under Taft excitation.

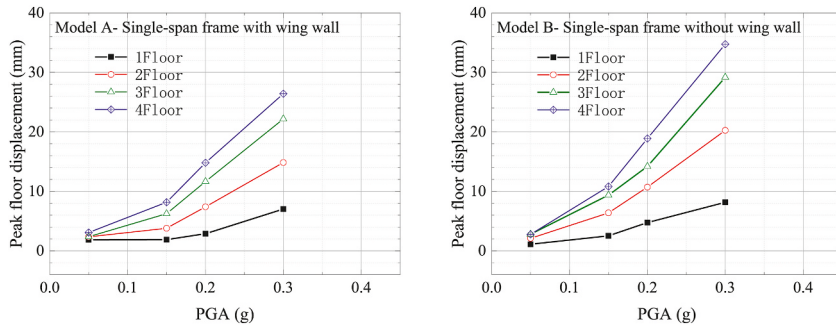


Fig. 28. Peak floor displacements versus PGA under Wolong excitation.

based earthquake), the average maximum IDR of Model-A was 1/244, indicating slight damage occurred to the frame retrofitted by wing wall, while the average maximum IDR of Model-B was 1/124, which demonstrates damage of the frame without retrofitting was moderate. When input PGA was 0.30g (rare earthquake), the average maximum IDR of Model-A was 1/69, indicating moderate damage occurred to the frame retrofitted by wing wall. In contrast the average maximum IDR of Model-B was 1/47, which demonstrates the damage of the frame without retrofitting was severe.

After the input PGA reached 0.4 g, the maximum IDR of Model-B was 1/23. Serious macro damage was observed, and penetrating cracks were observed on Model-B, which was on the verge of collapse. In contrast, the maximum IDR of Model-A was 1/37, approximately only 60% of that of Model-B. Most of the seismic damage was concentrated in the joints of the wing wall and beams, whereas the columns suffered minor damage, and the seismic capacity of Model-A was not lost.

4.2.3. Comparison of acceleration responses of the two specimens

The time history of the acceleration response was measured using the accelerometers on each floor. For simplicity, only the acceleration time history of the two specimens subjected to the El Centro wave under PGA of 0.15 g–0.40 g are presented in Figs. 31–34.

From Figs. 31–34 listed above, it can be seen that the basic trend of the floor acceleration time history for the two specimens approximates that of the time history of the shaking table. Generally, the higher the floor elevation, the greater the peak floor acceleration (PFA) [33]; however, the PFA on the third floor of Model-A is slightly lesser than that on the second floor when PGA is 0.40 g. Such a situation also occurs with Model-B when the input PGA is 0.30 g and 0.40 g. It is worthy to note that the PFAs of the four storeys for each specimen did not occur simultaneously.

Acceleration amplification factor (AAF) is defined as the maximum structural acceleration response divided by the maximum acceleration at the base [34]. The AAF was adopted in this study to describe the dynamic amplification effects in the shaking table test. The AAFs of different storeys of the two specimens in the tests are shown in Fig. 35.

As shown in Fig. 35, the AAFs are greater than 1.0 for all storeys when the PGAs of the excitations are less than 0.15 g. However, the AAF on the third floor for Model-A are less than 1.0 when the input PGA of Taft/Wolong was 0.2 g or 0.3 g. For Model-B, the AAF on the first and third floor approached 1.0 when the PGA of El Centro was 0.3 g or 0.4 g, and the AAF on the second and third floor approached 1.0 when the PGA of Taft or Wolong was 0.30 g. The AAFs are less than 1.0 when the PGA of Taft was 0.4 g.

From the amplification factors in Fig. 35, it can be seen that the amplification effect of Model-A is larger than that of Model-B. In Fig. 35(a) and (b), the AAF of Model-A is greater than 1.0 and the AAF in the fourth storey (roof) was much greater than that in the lower storeys. For Model-B, the AAF in the first and third storeys approaches 1.0 when the PGA is 0.3 g or 0.40 g. From Fig. 35(c) and (d), only the AAF in the third storey for Model-A is less than 1.0 when the input PGA of Taft is 0.2 g or 0.3 g. For Model-B, the AAF of the third storey approached 1.0 when the PGA was 0.2 g, and the AAFs of all the storeys were less than 1.0 when the PGA was greater than 0.20 g. The earthquake force cannot be transferred to the upper storeys because of the damage to the lower storeys for Model-B in the tests at 0.3 g and 0.4 g. From Fig. 35(e) and (f), we can also see that the AAFs in the third storey for Model-A are less than 1.0 when the

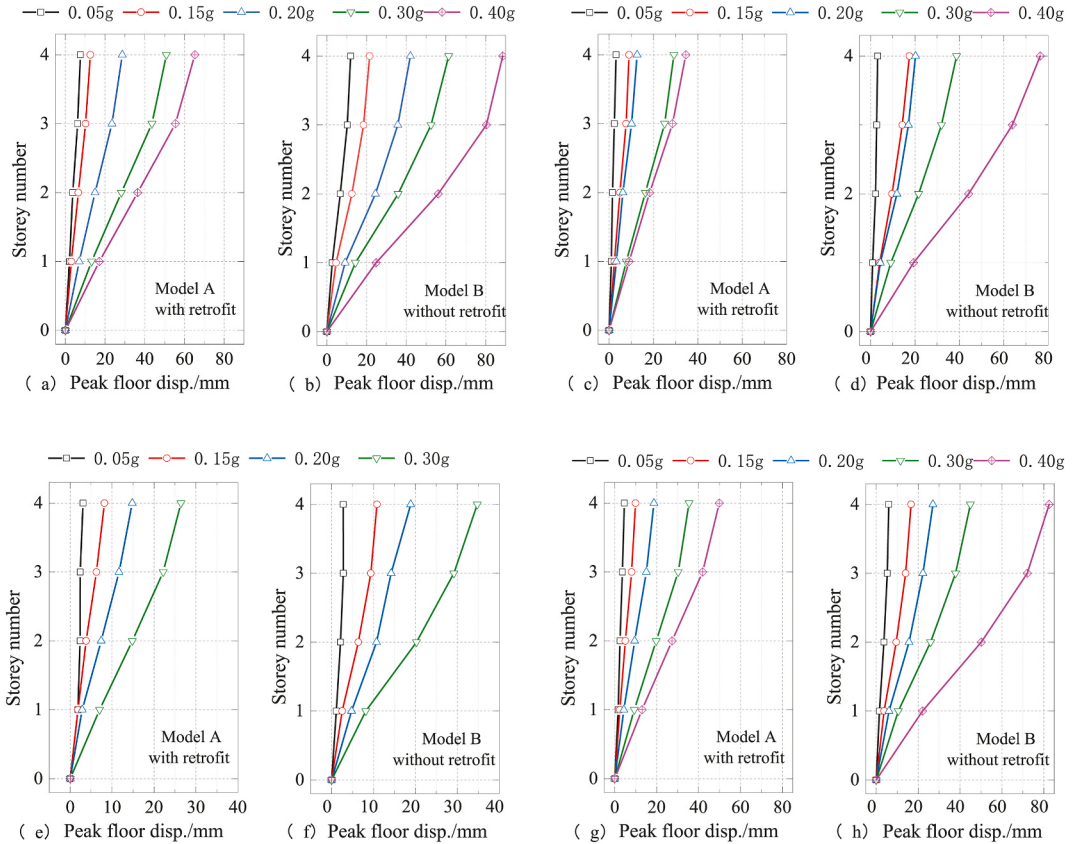


Fig. 29. Peak floor displacements (PFD) (a, c, e, g show the PFD of the frame with retrofit under El Centro, Taft, and Wolong excitons, and the average PFD, respectively; b, d, and f h show the PFD of the frame without retrofit under El Centro, Taft, and Wolong excitons, and the average PFD, respectively.

Table 12
Inter-storey drift ratio under different seismic actions.

Load case		A (with wing wall retrofit)				B (without wing wall retrofit))			
		1 F	2 F	3 F	4 F	1 F	2 F	3 F	4 F
0.05 g	El Centro	1/351	1/441	1/294	1/512	1/269	1/178	1/202	1/422
	Taft	1/728	1/1311	1/861	1/925	1/764	1/550	1/1421	1/1605
	Wolong	1/752	1/768	1/711	1/1258	1/623	1/601	1/779	1/1013
0.15 g	Average	1/540	1/692	1/503	1/783	1/453	1/330	1/433	1/754
	El Centro	1/242	1/201	1/198	1/302	1/155	1/91	1/122	1/235
	Taft	1/299	1/291	1/259	1/528	1/176	1/128	1/157	1/224
0.20 g	Wolong	1/382	1/377	1/294	1/375	1/285	1/186	1/242	1/495
	Average	1/297	1/271	1/244	1/381	1/192	1/124	1/161	1/279
	El Centro	1/104	1/90	1/84	1/139	1/78	1/47	1/64	1/113
0.30 g	Taft	1/220	1/243	1/184	1/286	1/163	1/97	1/139	1/223
	Wolong	1/250	1/159	1/169	1/228	1/151	1/121	1/207	1/153
	Average	1/165	1/139	1/129	1/199	1/117	1/75	1/109	1/151
0.40 g	El Centro	1/55	1/48	1/47	1/99	1/50	1/33	1/43	1/81
	Taft	1/93	1/84	1/83	1/173	1/79	1/57	1/70	1/106
	Wolong	1/103	1/92	1/98	1/170	1/88	1/60	1/81	1/129
Average	El Centro	1/78	1/69	1/69	1/138	1/68	1/47	1/60	1/102
	Taft	1/42	1/37	1/38	1/73	1/29	1/23	1/30	1/88
	Average	1/55	1/50	1/49	1/91	2/65	1/26	1/33	1/69

input PGA is 0.30 g. However, for Model-B, the AAF of the first storey approaches 1.0 when the input PGA is 0.15 g, and the AAF of the second and third storeys is less than 1.0 when the input PGA is 0.30 g. This is why the top ends of the columns in the first and second storey are cracked in the tests with inputs of 0.2 g and 0.3 g. The acceleration response coincides with the damage observed during the test.

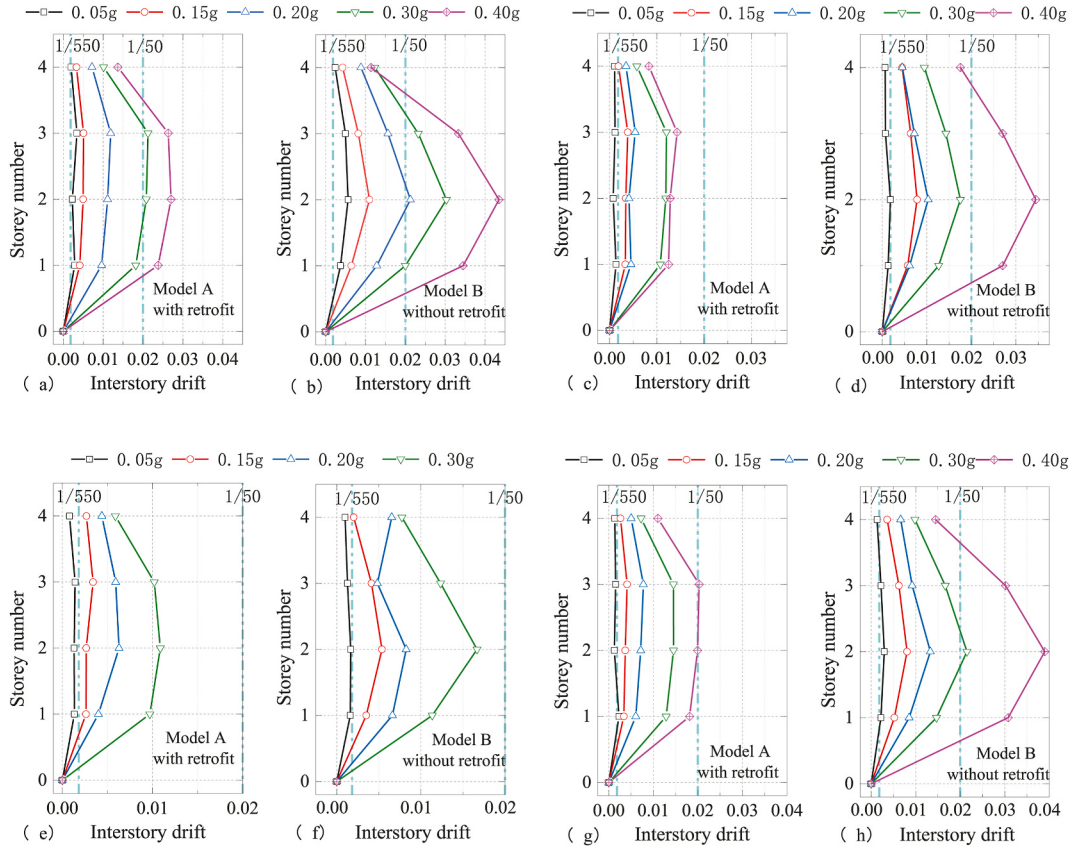


Fig. 30. The maximum inter-storey drift ratio (a, c, e, and g show the IDR of the frame with retrofit under El Centro, Taft, and Wolong excitations, and the average IDR, respectively; b, d, f, and h show the IDR of the frame without retrofit under El Centro, Taft, and Wolong excitons, and the average IDR, respectively).

Table 13
Structural limit states and corresponding maximum IDR [4,32].

Limit states	minor	moderate	severe	collapse
Maximum IDR	1/500	1/200	1/50	1/25

Note: The data in the table is the lower limit of the corresponding damage state.

Table 14
Damage states of the two specimens under three level earthquake action.

Earthquake action	0.05 g (Frequent Eq.)		0.15 g (DBE)		0.30 g (Rare Eq.)		
	Specimens	Model-A	Model-B	Model-A	Model-B	Model-A	Model-B
Average maximum IDR	1/503	1/330	1/244	1/124	1/69	1/47	
Damage states	none	minor	minor	moderate	moderate	severe	

5. Conclusions

To verify the effectiveness of retrofitting a single-span RC frame with wing walls, the retrofit scheme using wing walls for a single-span RC frame structure was determined by numerical simulation. Comparative shaking table tests were conducted on two large-scale models representing single-span RC frame structures with and without wing wall retrofitting, which were placed on the same shaking table board and tested simultaneously. According to the numerical analyses and experimental results, the following conclusions were drawn:

- (1) From the perspective of the retrofit scheme, the bidirectional retrofit scheme with wing walls for a single-span frame structure is a reasonable retrofit method because the wing walls are arranged in both directions so that the seismic capacity in both directions can be improved. Therefore, adding wing walls to a single-span frame in bi-direction is recommended.

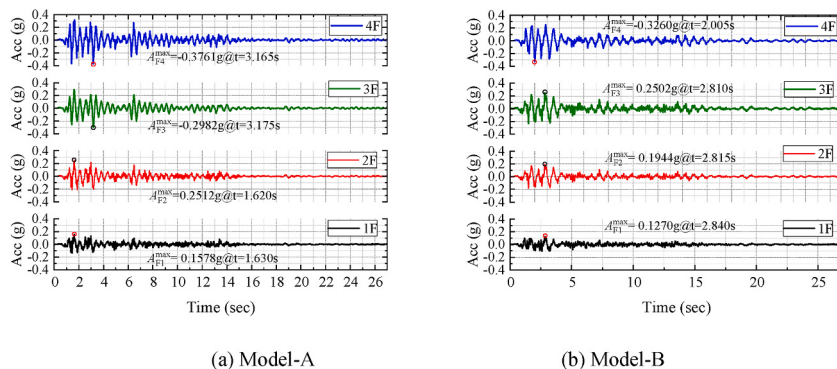
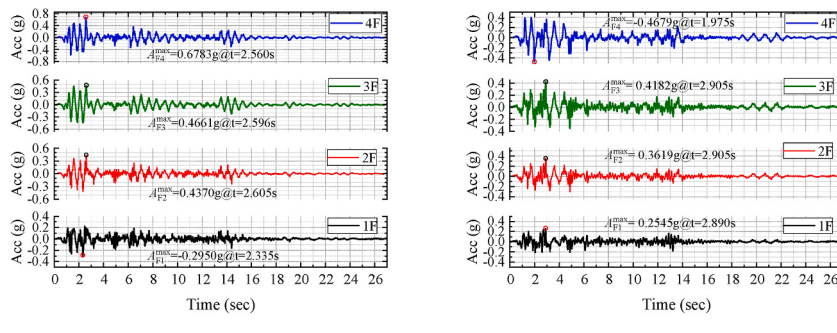


Fig. 31. Time histories of the acceleration responses of the two specimens under $\text{PGA} = 0.15 \text{ g}$.



(a) Model-A (b) Model-B

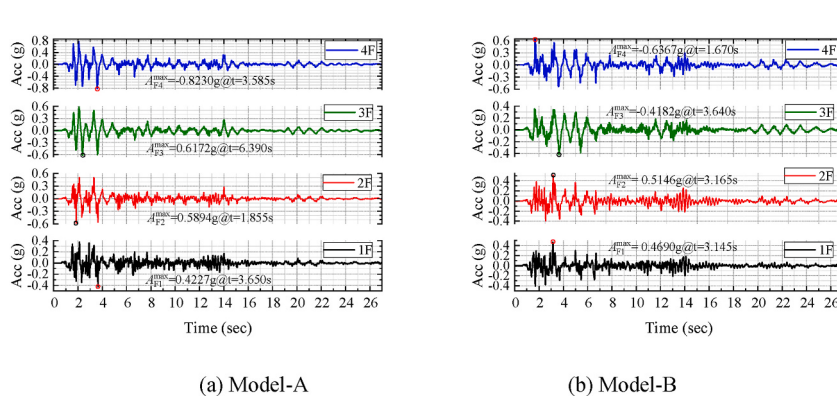


Fig. 33. Time histories of the acceleration responses of the two specimens under $\text{PGA} = 0.30 \text{ g}$.

- (2) From the perspective of dynamic property, it can be seen that the lateral resisting stiffness of the retrofitted frame is twice larger than that of the frame without retrofitting. Beside the seismic capacity of the single-span frame are improved by adding wing walls. The first indicator is that the frequency of the frame with retrofit stayed unchanged after an input PGA of 0.05 g; however, the frequency of the frame without retrofit decreased by approximately 5%. The second indicator is that the first frequency of the frame without retrofit decreased rapidly for a PGA of 0.15 g, while for a PGA of 0.20 g in the frame with retrofit, it decreased rapidly. In addition, after an input PGA of 0.40 g, the frequency of the frame with retrofit decreased significantly, while that of the frame without retrofit decreased only by a small amount, which demonstrated that the frame without retrofit reached its ultimate loading state; in contrast, there was still redundancy in the frame with retrofit.
 - (3) By comparing the damage phenomena of the two specimens, it can be seen that adding wing wall can increase the redundancy of the structure, and act as the first seismic line of defence. For the single-span frame without retrofit, cracks appeared in the early stages and rapidly developed, resulting in penetrating cracks at the ends of the beams and columns and forming beam and

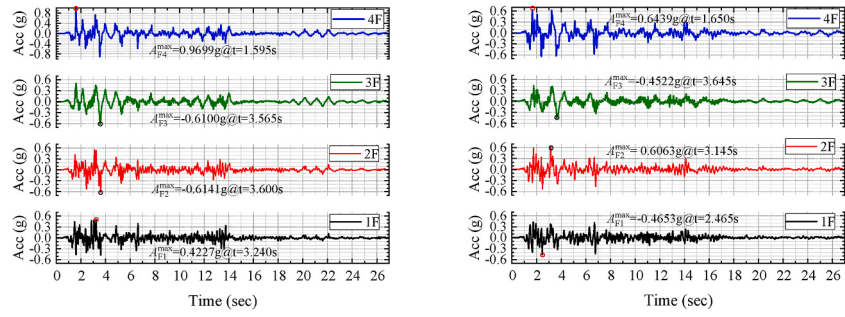


Fig. 34. Time histories of the acceleration responses of the two specimens under $PGA = 0.40$ g.

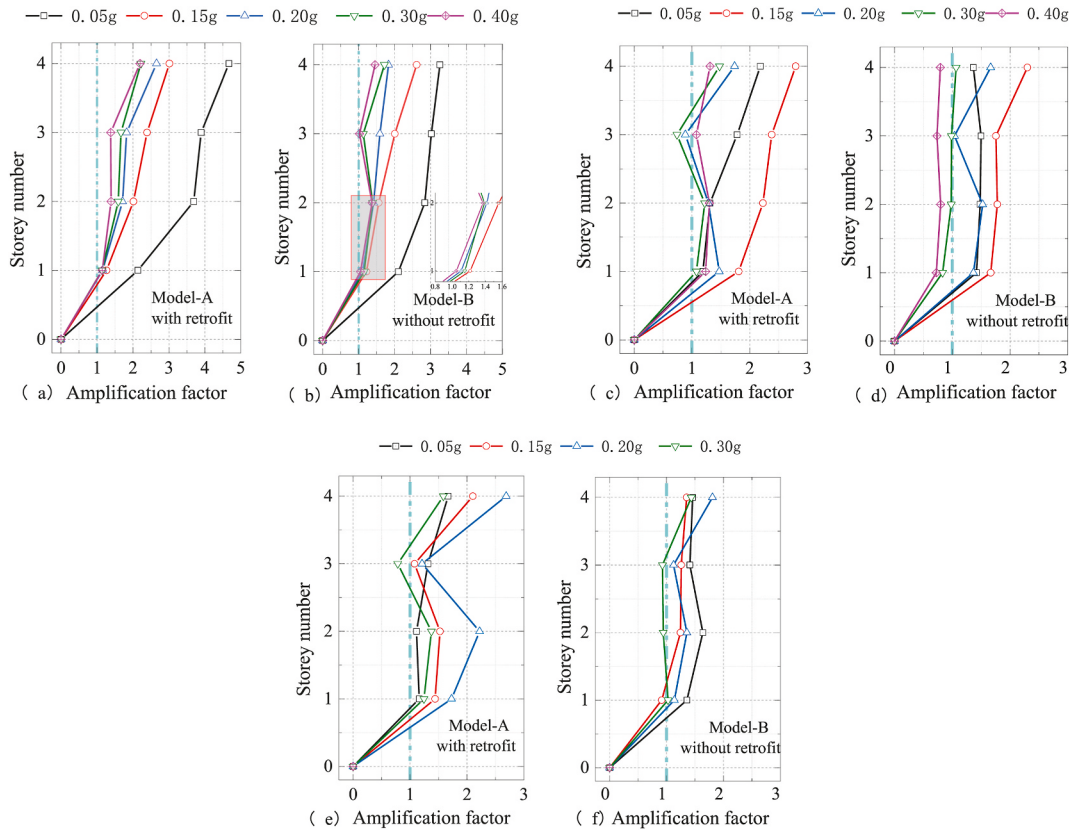


Fig. 35. AAF envelope curves of the two specimens (a, c, and e show the AAF of the frame with retrofit under El Centro, Taft, and Wolong excitations, respectively; b, d, and f show the AAF of the frame without retrofit under El Centro, Taft, and Wolong excitations, respectively).

column plastic hinges. Under such circumstances, the single-span frame will soon reach its ultimate capacity and collapse owing to the domino effect. For the single-span frame with retrofit, cracks first appeared in the construction joints between the wing walls and beams, and then extended to the wing walls and beams with increasing excitation. The cracks were evenly distributed over the entire beam rather than concentrated at the beam ends, and the structural ductility and energy dissipation were improved.

- (4) From a comparison of the measured response data, it can be seen that when subjected to the same level of ground motion, the peak floor displacement response of the frame retrofitted by wing wall reduced by 30%–40% compare with that of the frame without retrofitting. On average, the maximum IDR of the frame without retrofitting reached 1/47 (exceeded 1/50) when the seismic excitation is 0.30 g, while that of the frame retrofitted by wing wall just reaches 1/49 when the seismic excitation is 0.40 g . Therefore, the structure retrofitted by wing wall proved to be better in terms of its seismic performance.

(5) According to experimental phenomena and observational data, seismic performance of the single-span frame was improved by adding wing wall to the frame. When input PGA was 0.15g (design based earthquake), slight damage occurred to the frame retrofitted by wing wall, while damage of the frame without retrofitting was moderate. When input PGA was 0.30g (rare earthquake), moderate damage occurred to the frame retrofitted by wing wall, while damage of frame without retrofitting was severe. Therefore, adding wing walls is an effective method for retrofitting single-span RC frame structures.

CRediT authorship contribution statement

Lingxin Zhang: Conceptualization, Funding acquisition, Supervision. **Caiquan Wang:** Data curation, Investigation, Software, Writing – original draft. **Yongsheng Chen:** Formal analysis, Methodology, Validation, Visualization, Writing – review & editing.

Declaration of competing interest

The authors declare that they have no known competing financial interests or personal relationships that could have appeared to influence the work reported in this paper.

Data availability

The data that has been used is confidential.

Acknowledgements

The research reported here was sponsored by “Joint Fund of Earthquake and National Natural Science Foundation of China under Grants No. U2139209, Natural Science Foundation of Heilongjiang Province under Grants No. LH2022E123, Scientific Research Fund of Institute of Engineering Mechanics, China Earthquake Administration under Grant No. 2022C06, No. 2019D18”.

References

- [1] K.C. Tsai, C.P. Hsiao, M. Bruneau, Overview of building damages in 921 Chi-Chi earthquake, *Earthquake Engineering and Engineering Seismology* 2 (1) (2000) 93–108.
- [2] Y. Wang, Lessons learned from the “5.12” Wenchuan Earthquake: evaluation of earthquake performance objectives and the importance of seismic conceptual design principles, *Earthq. Eng. Vib.* 7 (3) (2008) 255–262.
- [3] PRC National Standard (GB50223-2008), Standard for Classification of Seismic Protection of Building Constructions[S], China Architecture and Building Press, Beijing, 2008 (in Chinese).
- [4] PRC National Standard (GB50011-2010), Code for Seismic Design of Buildings[S], China Architecture and Building Press, Beijing, 2010 (in Chinese).
- [5] Xie Xianxin, Pan Yi, Kou Chuangqi, Zhang Lingxin, Zhu Baijie, Typical seismic damage investigation and analysis to school buildings in the Luding Ms 6.8 earthquake, *Earthquake Engineering and Engineering Dynamics* 42 (6) (2022) 12–24 (in Chinese).
- [6] W. Yang, X. Guo, W. Xu, et al., Wing walls for enhancing the seismic performance of reinforced concrete frame structures, *Earthq. Eng. Eng. Vib.* 15 (2) (2016) 411–423.
- [7] M.C. Guo, S.G. Luan, Y. Ju, et al., Study on seismic behavior of reinforced concrete short column with flange wall, *J. Build. Struct.* 17 (3) (1996) 32–42 (in Chinese).
- [8] T. Kabeyasawa, Y. Kim, et al., Tests on reinforced concrete columns with wing walls for hyper-earthquake resistant system[C], in: Proceedings of 3rd International Conference on Advances in Experimental Structural Engineering, October 2009. San Francisco, USA.
- [9] T. Kabeyasawa, Y. Kim, M. Sato, et al., Tests and analysis on flexural deformability of reinforced concrete columns with Wing Walls, Proceedings of the 2011 Pacific conference on earthquake engineering (PCEE2011), New Zealand Society for Earthquake Engineering, Paper 102 (2011) 1–8.
- [10] K.C. Liu, Y.W. Liu, W.C. Huang, et al., The structure behavior of reinforced concrete wing-wall under earthquake, *Int. J. Phys. Sci.* 5 (7) (2010) 1164–1174.
- [11] S.H. Yin, S.Y. Chang, W.I. Liao, et al., Experimental study on seismic retrofit of RC column with wing wall in Taiwan and Japan, in: Proceedings of the International Symposium on Engineering Lessons Learned from the 2011 Great East Japan Earthquake, March 1–4, 2012. Tokyo, Japan.
- [12] S.Y. Chang, T.W. Chen, N.C. Tran, et al., Seismic retrofitting of RC columns with RC jackets and wing walls with different structural details, *Earthq. Eng. Eng. Vib.* 13 (2) (2014) 279–292.
- [13] S. Suzuki, H. Kuramoto, Effects of shear-span-ratio and axial force on structural performance of CES columns with wing wall, in: 16th World Conference on Earthquake Engineering, Santiago Chile, 2017. January 9th to 13th.
- [14] Y. Li, Y. Sanada, K. Maekawa, A practical method for strengthening repairing poorly detailed RC beam-column joints in developing countries: installing wing walls to existing columns, in: 16th World Conference on Earthquake Engineering, Santiago Chile, 2017. January 9th to 13th.
- [15] M.N. Rahman, T. Yamakawa, Experimental and analytical investigation of seismic retrofit for one-sided wing-wall RC columns, *Proceedings of the Japan Concrete Institute* 26 (2004) 1351–1356.
- [16] T. Yamakawa, M.N. Rahman, Y. Morishita, Experimental investigation and analytical approach for seismic retrofit of RC column with wing-wall, *Journal of Structural and Construction Engineering* 608 (2006) 109–117. AJ.
- [17] Huang SJ, Zhang HB. Study on seismic behavior of nonductile frame retrofitted with RC wing walls(II) [J].Technical Report NCREE-03-046, National Center for Research on Earthquake Engineering, Taiwan.(In Chinese).
- [18] M.Y. Klatakci, G. Yavuz, An experimental study on strengthening of vulnerable RC frames with RC wingwalls, *Struct. Eng. Mech.* 41 (6) (2012) 691–710.
- [19] T. Kabeyasawa, T. Mukai, H. Fukuyama, et al., Full-scale static loading test on a five story reinforced concrete building (part1: outline of the test), in: 16th World Conference on Earthquake Engineering, Santiago Chile, 2017. January 9th to 13th.
- [20] Y.T. Bai, G.L. Bai, Pseudo-dynamic and quasi-static testing of an irregular steel concrete composite frame with wing walls, *Int. J. Struct. Stabil. Dynam.* 16 (2) (2016) 1450095.
- [21] Y. Kim, T. Kabeyasawa, T. Matsumori, et al., Numerical study of a full-scale six-story reinforced concrete wall-frame structure tested at E-Defense, *Earthq. Eng. Struct. Dynam.* 41 (8) (2012) 1217–1239.
- [22] PRC National Standard (GB50099-2011), Code for Design of School [S], China Architecture and Building Press, Beijing, 2011 (in Chinese).
- [23] PRC National Standard (GB50011-2001), Code for Seismic Design of Buildings[S], China Architecture and Building Press, Beijing, 2001 (in Chinese).
- [24] PRC National Standard (GB50010-2010), Code for Design of Concrete Structures[S], China Architecture and Building Press, Beijing, 2010 (in Chinese).
- [25] PRC Industry standard (JGJ3-2010), Technical Specification for Concrete Structures of Tall Building [S], China Architecture and Building Press, Beijing, 2010 (in Chinese).
- [26] MIDAS user manual. http://manual.midasuser.com/building/cn-na/chapter_2/2_4/2.4.1.htm. (Accessed 13 February 2024).

- [27] L.X. Zhang, C.Q. Wang, J.P. Liu, Analysis of the influence on structural seismic capability by wing wall strengthening method, *China Civ. Eng. J.* 41 (8) (2012) 1217–1239 (in Chinese).
- [28] C.S. Li, S.S.E. Lam, M.Z. Zhang, et al., Shaking table test of a 1:20 scale high-rise building with a transfer plate system, *J. Struct. Eng.* 132 (11) (2006) 1732–1744.
- [29] X. Lu, G. Fu, W. Shi, et al., Shake table model testing and its application, *Struct. Des. Tall Special Build.* 17 (1) (2010) 181–201.
- [30] M. Dolce, D. Cardone, F.C. Ponzo, C. Valente, Shaking table tests on reinforced concrete frames without and with passive control systems, *Earthq. Eng. Struct. Dynam.* 34 (2005) 1687–1717, <https://doi.org/10.1002/eqe.501>.
- [31] PRC National Standard (GB/T 24335-2009), Classification of Earthquake Damage to Buildings and Special Structures [S], China Earthquake Press, Beijing, 2009 (in Chinese).
- [32] FEMA273 NEHRP Guidelines for the Seismic Rehabilitation of Buildings, Building Seismic Safety Council, Washington, D.C, 1997.
- [33] P. Quintana Gallo, U. Akguzel, A.J. Carr, et al., Seismic response of a non-ductile RC frame building subjected to shake-table excitations, *Bull. Earthq. Eng.* 20 (2022) 517–545, <https://doi.org/10.1007/s10518-021-01228-4>.
- [34] M. Gong, Z. Zuo, X. Wang, et al., Comparing seismic performances of pilotis and bare RC frame structures by shaking table tests, *Eng. Struct.* 199 (2019) 109442.